A STANDARDIZED METHOD FOR 3D CAROTID ARTERY IMAGING USING FREEHAND ULTRASOUND SCANNING

by

Rumman Mahmud
A Thesis
Submitted to the
Graduate Faculty
of
George Mason University
in Partial Fulfillment of
The Requirements for the Degree
of
Master of Science
Computer Engineering

Committee:

Dr. Siddhartha Sikdar, Thesis Director

KGaj Dr. Kris Gaj, Committee Member

VIkonomidou Dr. Vasiliki Ikonomidou, Committee Member

Dr. Andre Manitius, Department Chair

Dr. Lloyd J. Griffiths, Dean, Volgenau School of Engineering

Date: 12/09/2011

Fall Semester 2011
George Mason University
Fairfax, VA

A Standardized Method for 3D Carotid Artery Imaging Using Freehand Ultrasound Scanning

A thesis submitted in partial fulfillment of the requirements for the degree of Master of Science at George Mason University

By

Rumman Mahmud
Bachelor of Science
George Mason University, 2002

Director: Siddhartha Sikdar, Assistant Professor
Department of Electrical and Computer Engineering

Fall Semester 2011
George Mason University
Fairfax, VA

Table of Contents

Page

List of Tables

List of Figures

Abstract

A STANDARDIZED METHOD FOR 3D CAROTID ARTERY IMAGING USING FREEHAND ULTRASOUND SCANNING

Rumman Mahmud, M.S.

George Mason University, 2011

Thesis Director: Dr. Siddhartha Sikdar

Stroke is the third leading cause of death in USA and second leading cause worldwide. Current diagnosis of stroke involves ultrasound duplex Doppler examination of the carotid arteries, which gives information on the severity of luminal stenosis caused by atherosclerotic plaque. Recent research shows that rupture-prone carotid plaques associated with stroke not only narrow the artery lumen, but by progress along the artery wall as well, thus the total plaque burden may be of clinical significance. This thesis presents a standardized system to enable reproducing carotid artery plaque volumes so that the progression can be monitored in longitudinal studies using freehand 3D Ultrasound (US) grayscale imaging. Two aims of this work are to develop methods to reproduce freehand US scanned images and to reconstruct the 3D plaque volume. The system integrates US imaging and an electromagnetic position tracking device to guide

the observer of the study to reproduce the US image, the position of the study subject in longitudinal studies, and the 3D position and orientation of ultrasound image frames to reconstruct the carotid plaque volume.

Positioning accuracy was found to be around 7.09±2.32mm. Calibration of the images was done using a string phantom with 1.39 mm, 1.36mm, 1.37mm, 1.42mm, and 1.43mm accuracy for depth settings from 35mm to 55mm in 5mm increment. Reconstruction of the volume was performed using a software application called Stradwin.

Chapter 1. Introduction

This thesis presents the development of a standardized system to enable quantification of carotid artery atherosclerotic plaque progression for longitudinal studies using Ultrasound (US) grayscale imaging. The long-term goal is to utilize these methods to identify artery plaque that is more likely to rupture and cause stroke.

Stroke is the third leading cause of death in the United States of America (USA) [59] and second worldwide [60]. There are two types of stroke: ischemic and hemorrhagic. An ischemic stroke is caused by atheroembolic or thromboembolic debris blocking a blood vessel in the brain, whereas a hemorrhagic stroke is caused by a rupture of a blood vessel in the brain. The vast majority of strokes (87% of the strokes in USA) are ischemic strokes [63]. The embolic material may be produced by plaque rupture or blood clot formation in some part of the body, typically the heart, which then travels through the arterial bloodstream and reaches the narrow brain arteries. Almost one fourth of the embolic strokes (20% to 30%) come from debris originating from plaque build-up in the carotid arteries [58].

The North American Symptomatic Carotid Endarterectomy Trial (NASCET) [65] indicated that surgical endarterectomy in patients with more than 70% carotid stenosis has possible benefits in terms of reducing the risk for stroke. Therefore, current clinical management is based on determining the severity of stenosis. Patients with 70% arterial stenosis undergo standard revascularization procedures--stent or endarterectomy--to avoid stroke risk. The diagnostic method of choice for determining carotid stenosis severity is ultrasound (US) duplex Doppler imaging. The severity of the stenosis is determined based on the peak blood velocity through the narrowest lumen. Criteria have been developed to determine the percentage narrowing based on the blood velocity. However, in recent years, research has shown that there may be other features of carotid plaque that are vulnerable to rupture. It has been found that major criteria for a plaque to be vulnerable include thin fibrous cap, large lipid core, and rapid progression [47]. The stenosis may build up along the vessel wall, and be vulnerable, without a significant luminal narrowing [49]. Thus, a lower degree of plaque can still be at a high risk of rupturing. There are currently no standardized methods to determine stenosis progression and plaque architecture using ultrasound.

A sophisticated diagnostic procedure should be able to detect a vulnerable plaque (even <70% stenosis) or refrain patients from undergoing pre-emptive surgical procedures (>70% stenosis, but may not be vulnerable). While duplex Doppler can be used to quantify the tightest luminal narrowing, it provides no information about the extent of atherosclerotic disease or the plaque burden.

Our approach to understanding the progression of vulnerable carotid plaque is to quantify the three dimensional plaque volume and gray scale plaque characteristics over time. The appearance of carotid plaque on grayscale imaging is prone to variability due to differences in insonation angles, neck position, and cardiac and respiratory cycle. A magnetic tracking device is being used in this thesis to be able to reproduce the probe angle relative to the anatomy and the head position of the patient. These methods can be expanded in the future to track cardiac and respiratory variability.

I. Literature Review

Reproducibility of freehand 3D ultrasound includes three major factors: reproducing the head or neck position, spatial calibration of the ultrasound images, and reconstructing the 3D volume. The subject’s head position and orientation play a vital role in the carotid artery geometry [2]. Monitoring the head position becomes essential when the US images need to be compared with a previously scanned image. Molinari et al. have used a Meijer’s arc [45] to create reproducibility in US scan. However, there are several disadvantages to the Meijer’s arc. The Meijer's arc might be inconvenient for a patient to wear it around the neck. Also, the arc measures head rotation to the left or right of the midline in the transverse plane; but cannot detect an angle created due to neck extension flexion in the sagittal plane or neck rotation in the coronal plane. To correct for this Allott et al. used a custom mechanical frame that touches the subject’s forehead and cheek, thus fixing the head in a reproducible position/orientation [1]. The frame constrains the imaging views and may not allow the sonographer to obtain an optimal view of the carotid artery. A literature review did not reveal any studies that have used a tracking sensor on the subject to monitor their head posture to obtain reproducible US image of the carotid artery plaque.

There is a large body of literature on the use of freehand 3D ultrasound using position tracking devices on the Ultrasound probe [1]-[5]. A popular choice is to use a magnetic position tracking system to track the US probe position/orientation [66]. The probe position information is used to reconstruct a 3D volume from the US images. Calibration plays a vital role in 3D volume reconstruction from the ultrasound images. Calibration provides the information of the correct position of an image pixel into the volume. There are three most common methods used to perform the calibration process. First, by scanning different types of string planes then reconstructed positions can be compared to hand measurements of the string positions. Second, by scanning a bead point from different probe orientation. Third, by using a custom phantom with known object or shape in it that would help calculating the relationship between the scanned images and the volume. When choosing a calibration method one should consider the accuracy, reliability, and ease of obtaining the data. Poon et al. showed three calibration methods using IXI-shaped wire phantom, a cube phantom and a stylus [38]. The performance of the IXI-shaped wire phantom on calibration reproducibility, point accuracy and reconstruction accuracy by distance measurement was found to be the best among three. Bergmeir at al. compared calibration performance of the tracked phantom’s (TP) spatial location to the calibration scans to the scans taken from multiple perspectives using hand–eye calibration methods [32].

Researchers have used different technologies for tracking devices for the 3D volume reconstruction. A choice of the tracking device technology depends on the research environment. An optical tracking device is more accurate than an electromagnetic device. In a research environment where a direct line of vision from the transmitter to the sensors cannot be maintained, an optical tracking device may not be suitable. With an electromagnetic tracking device the direct line of vision does not have to be maintained, but it is highly sensitive to metal in the environment. Mercier et al. have compared the tracking technologies and different calibration methods chosen by the researchers [66].

II. Research Objectives

This thesis standardizes a method to enable quantification of carotid artery stenosis progression for longitudinal studies using freehand Ultrasound (US) grayscale imaging. Grayscale images will give information on the stenosis composition. As mentioned above, plaque architecture and composition holds vital information regarding vulnerability. To have a better understanding of the architecture and detect plaque progression, 3D volume will be reconstructed out of the 2D grayscale images. Furthermore, a freehand sweep enables to scan complex and large plaques that may span multiple artery segments.

As a part of the thesis, a software program has been developed that would monitor the US image, which is dependent on the US probe and the patient’s head posture. The software will also guide the patients to the same posture in the following visit, hence facilitating reproducibility in the imaging method. The system will also provide position and orientation information of each US image frame so that a 3D volume can be reconstructed from the freehand scanning.

Chapter 2. Materials

Two devices were used in this project: Sonix MDP Ultrasound machine (Ultrasonix Medical Corporation, British Columbia, Canada) and 3D Guidance TrakSTAR (Ascension Technology, VT, USA) electromagnetic tracking device. Descriptions of the devices and details of the operational setup are provided below.

I. Sonix MDP Ultrasound Machine

Sonix MDP is a diagnostic ultrasound system, which also offers a research interface. In research mode the device performs all clinical functionalities and it also lets custom applications to retrieve US image frame data in different formats. Raw or processed data can be retrieved in real-time or later to analyze the US image. The system provides several Software Development Kits (SDK) to build applications, such as Porta, Texo, Ulterius etc.

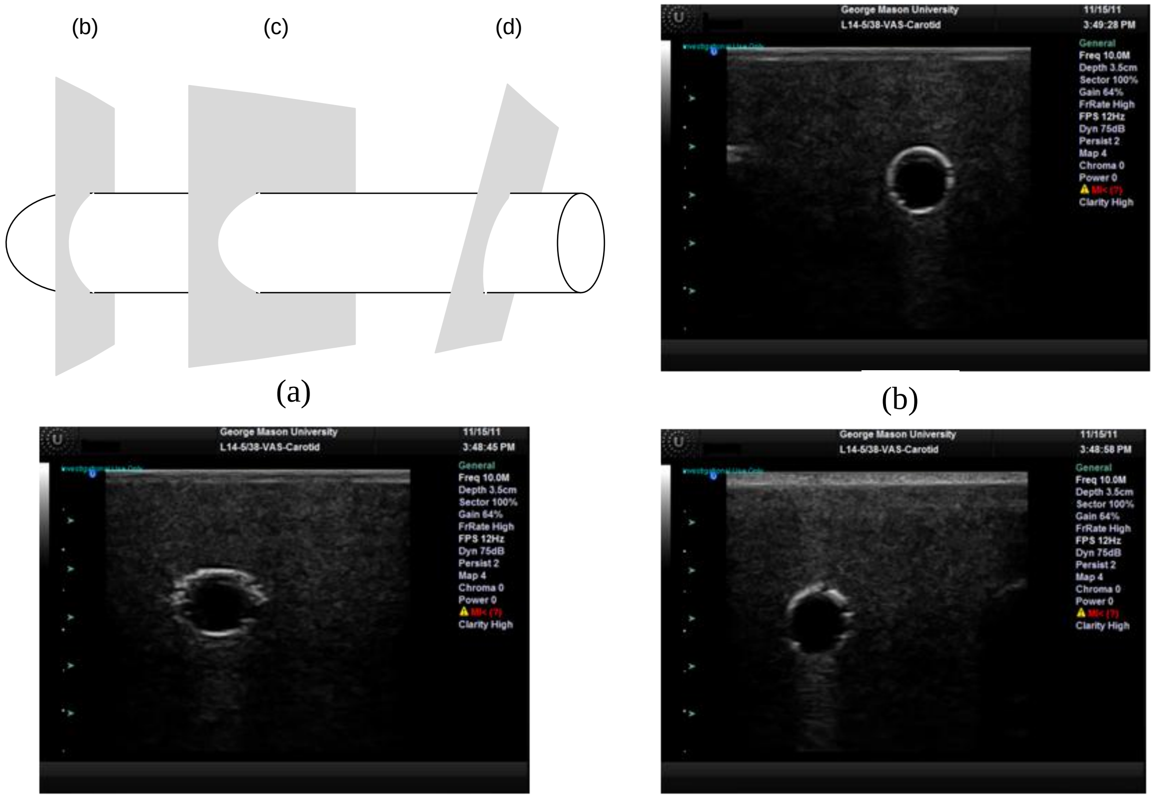

(a) (b)

(c) (d)

Figure 1: Ultrasound images with different probe orientation (a) showing image frame orientation on an tube shaped object that can simulate a carotid artery, (b) an image frame, the tube appears to be circle in an image, (c) rotating the probe makes the circle looks elongated, and (d) tilting the probe creates shadow under the circle and the bottom edge is blurred.

A 14MHz linear array transducer (L14-5/38) was used for freehand scanning. Ultrasound image is highly dependent on the angle insonation (Figure 1). In case of imaging a cylinder, if the probe's lateral axis is perpendicular with the cylinder's axis, the ultrasound image appears as a circle. The shape of the circle in the image can be changed by rotating the probe to have different orientation. A change in roll angle makes the circle to appear as an elongated eclipse (Figure 1c). Similarly, a pitch angle difference may blur the bottom edge of the cylinder image and enhance shadows underneath it (Figure 1d). A series of freehand scanned images can be stitched together to reconstruct the 3D volume image of the anatomy. Unlike Magnetic Resonance Imaging (MRI) or Computer Tomography (CT) frames, freehand US scanned frames are not uniformly spaced and aligned to each other. A complex calculation needs to be performed to the find out the contribution of an image pixel into a voxel.

II. Ascension 3D Guidance TrakSTAR

The thesis uses Ascension Technology's 3D Guidance TrakSTAR magnetic motion tracking system. The tracking system includes three components: an electronics unit (Figure 2), a transmitter, and four sensors. The electronics unit is the central component of the system that is connected to a PC running the custom software. This device synchronizes data between the transmitter and the sensors and communicates with the PC.

Figure 2: 3D Guidance electronics unit

The transmitter generates pulsed DC magnetic fields and it is very sensitive to metal. Hence, the transmitter should be placed on a non-metallic plane, such as a wooden or a plastic stand. The magnetic flux is picked up by coils inside a sensor. Each sensor has three coils inside it, each placed orthogonally to the other two. The magnetic flux is converted into electrical energy which is sent back to the electronics unit. The position and the orientation of a sensor are calculated from the relative intensity of the current generated by each of the sensor coils. The short range sensors that are being used in this project have cylindrical form with 2.0 mm diameter and 9.9 mm in length. Each sensor has its own X-Y-Z axes and has 6 Degrees of Freedom (6 DOF) in its movement. The sensor position (in mm) and orientation (in degree) are provided in respect to the transmitter's reference frame (Figure 3).

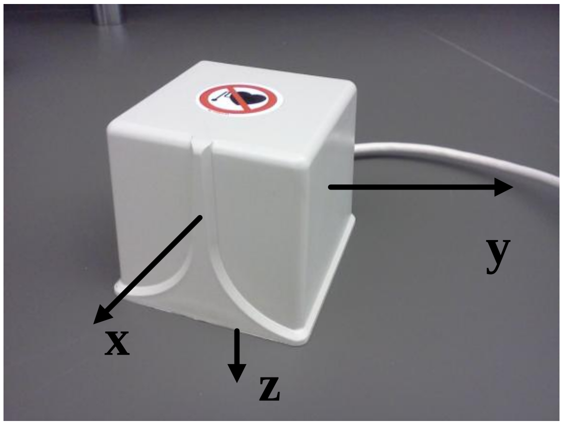

Figure 3: 3D Guidance transmitter

A sensor's position is calculated from the transmitter's reference frame. The sensor's orientation is the angular displacement of the sensor's axis from the transmitter's reference frame axis.

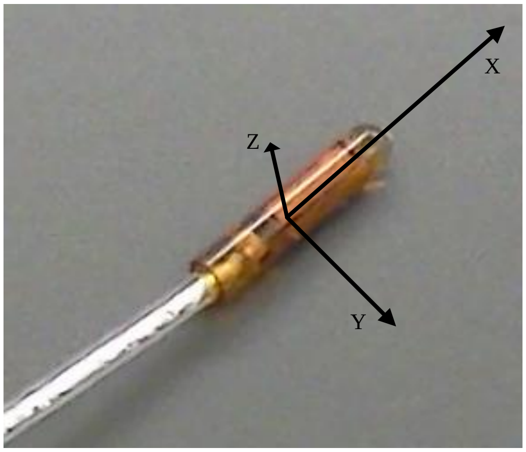

Figure 4: 3D Guidance sensor

This thesis follows orientation nomenclature using Euler angles: azimuth (a), elevation (e), and roll (r). The azimuth and roll values range between +180 and -180 degrees, whereas the elevation takes the value from -90 to +90 degrees. At ± 90 degrees of elevation, azimuth and roll become undefined per Euler angle characteristics.

The positive X-axis of a sensor comes out from the top of the sensor as shown in Figure 4. However, there is no physical identification of the Y and Z axes. The lack of the identification poses some complexity in figuring out the US image plane orientation and calculating the head posture. Sensors can be glued to a flat rigid body so that its orientation remains the same as the rigid body is attached to the patient. The *Operational Environment* section of this document provides more information on the sensor placements.

III. Operational Environment

The Sonix MDP is run in research interface mode and the tracking device is connected to the Sonix machine via a Universal Serial Bus (USB). The patient is scanned in supine position and the transmitter is placed close to the crown of the head facing front. A sensor (sensor 1) is attached on the probe and three sensors are placed on the subject to monitor the head position. It is assumed that sensor 1 will not be taken off from the probe, thus considered fixed permanently to the probe.

Two sensors are placed on the patient's forehead (sensor 2 and sensor 4) and one sensor is placed on the sternal notch (sensor 3). Sensor 3 was attached to a rigid body before attaching to the sternal notch using medical adhesive. The tip of sensor 3 pointed to the head of the patient. Sensor 2 was placed on the forehead followed by sensor 4 in a line (Figure 5); tips of these sensors were one and a half inches apart. The distance between Sensors 2 and 4 was recorded. In this thesis, these two sensors are put attached to a rigid body. During the application it should be noted that tip of sensor 2 is in-between the eyebrows and touching the upper line of the brows.

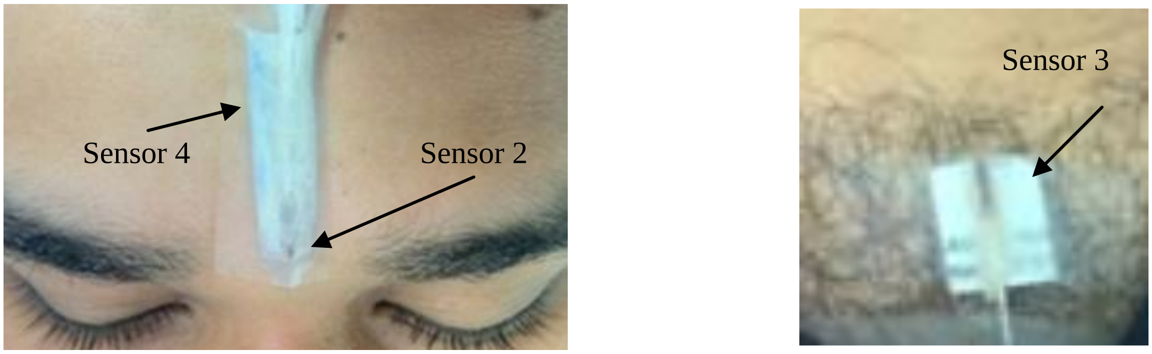

(a) (b)

Figure 5: Sensor placement on the patient

To calculate the head rotation in transverse, sagittal, and coronal planes, two sensor positions (sensors 2 and 4) were recorded. Their orientation data were not considered in the calculation.

Chapter 3. Methods

I. System Architecture

The system that was developed for this thesis monitors the subject's head posture and guides them to reproduce the position in the following visits. The secondary aim of the system was to get the position and the orientation of each US frame to reconstruct a 3D volume image. The system can be divided in three modules based on their functionalities: (1) Synchronized Data Collection, (2) Position Feedback System, and (3) 3D Reconstruction.

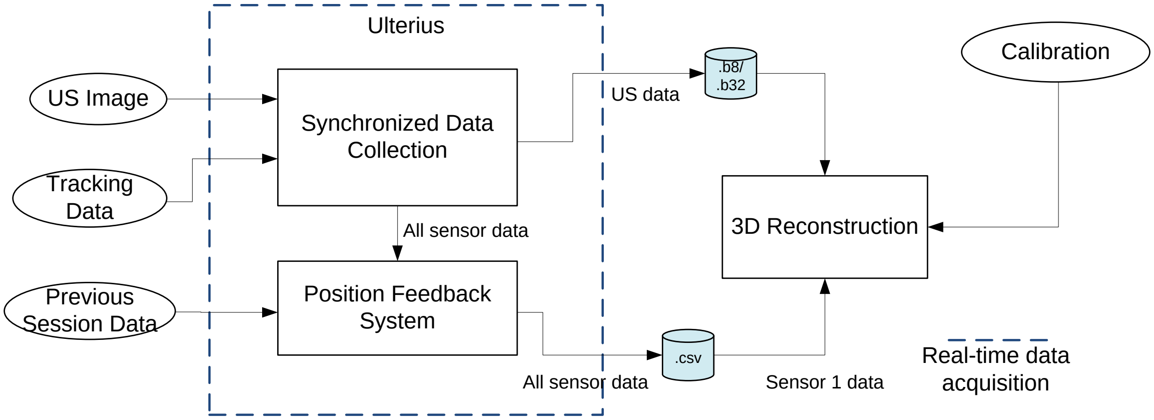

Figure 6: The system can be divided in three modules based on their functionalities: Synchronized Data Collection, Position Feedback System, and 3D Reconstruction. Synchronized Data Collection and Position Feedback System are performed by custom-built software. 3D volume reconstruction is done using Stradwin.

(1) Synchronized Data Collection: The data collection module constituents are interfaces of 3DGuidance trakSTAR and Ultrasound machine. Real-time US images were collected by a software application based on the Ulterius SDK. The application will be referred to as ‘Ulterius’ for readability purpose. Ulterius also handles tracking device communication and synchronizes the position data with the US image frames.

    The modules send out all the position data to the Position Feedback System in real-time. US data is stored in a file once the acquisition is done. These data will be post processed to reconstruct the 3D volume.

(2) Position Feedback System: The Position Feedback System is also a part of Ulterius. This is the user interface that guides a patient to reproduce their head position in a follow-up session. The position feedback was provided using either a plot by 3D Graph ActiveX control (National Instruments Corporation, Austin, TX) or numeric coordinate values.

Initially, the position feedback system utilized an ActiveX control plot. The plot showed real-time sensor positions on the forehead and the probe in reference of the manubrium (Figure 7). In case of a follow-up session, the previous positions were displayed as well. As shown in the figure below, sensor positions in the first visit are shown in red markers and the current positions are in green markers. To reproduce the position, the observer guided the patient to move the head to till the real time markers corresponding to the current session overlapped with the static markers corresponding to the previous session.

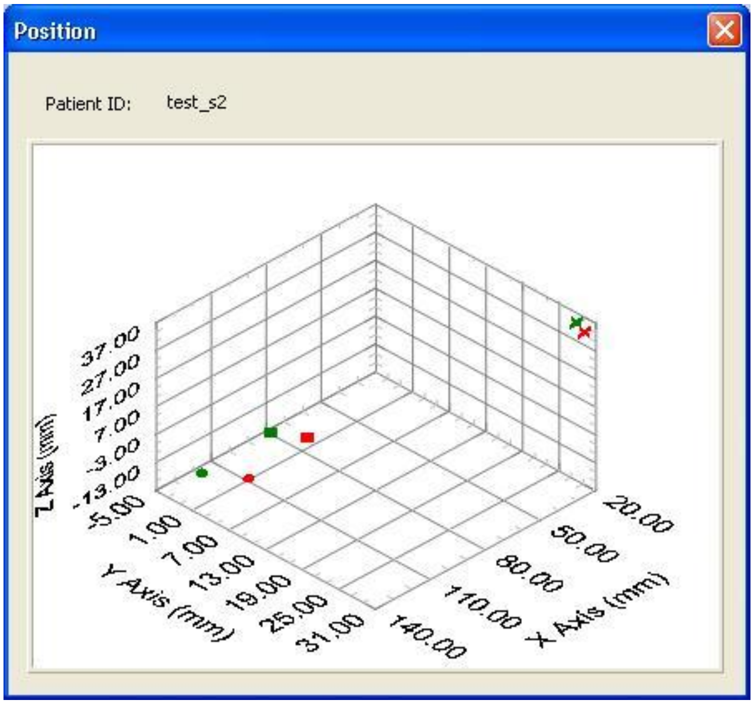

Patient ID: test_s2

Figure 7: ActiveX Graphical Plot

This method did not achieve the expected efficiency to guide the patient to the previously held position. To have a better performance the feedback system was changed to display numeric coordinate values for sensor 2 and 4 with respect to sensor 3 in a dialog box (Figure 8). Description of the dialog box is provided in Appendix A.

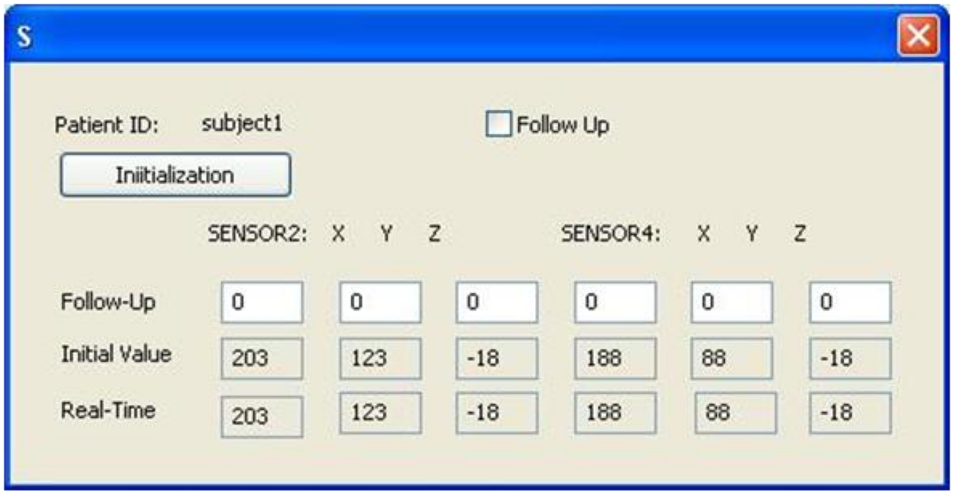

Patient ID: subject1

☐ Follow Up

	SENSOR2: X	Y	Z	SENSOR4: X	Y	Z
Follow-Up	0	0	0	0	0	0
Initial Value	203	123	-18	188	88	-18
Real-Time	203	123	-18	188	88	-18

Figure 8: Coordinate values

All of the sensor data were recorded in a file after acquiring data. Sensor 1 data were used in 3D volume reconstruction and all other sensor data assisted in reproducing the head position in a follow-up session.

(3) 3D Reconstruction: 3D volume reconstruction was performed from the data saved by Ulterius. Calibration plays a vital role in the reconstruction process. The calibration method has been described later in this chapter.

Stradwin was used for the volume reconstruction. It utilizes the US image data, probe’s position and orientation (sensor 1 was attached to the probe), and the calibration matrix as inputs.

II. System Functional Flow

The system was developed to be used in a clinical environment. A professional sonographer operated the system and scanned asymptomatic patients with more than 70% carotid artery stenosis. The system executed on a Sonix MDP machine. To control the image quality, the operator may use hardware controls of the US machine or the software interface provided by the system. For a follow-up visit, the observer is responsible to make sure the subject's head position matches with the previous visit.

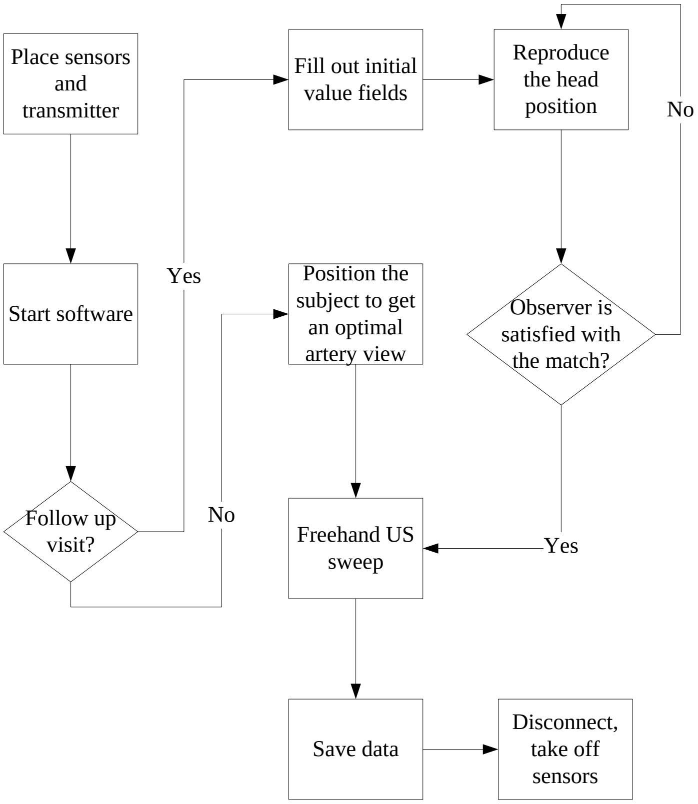

Figure 9: Flowchart of the system

Appendix A provides the protocol to use the system.

III. Alternate Implementations

As mentioned above, Sonix provides different SDKs to build custom applications. A similar application was developed using Porta. Real-time data can be acquired with Porta as well. A drawback of an application built on Porta is that the US image display needs to be created as well. Visualizing good quality of US image is not a trivial task. Furthermore, with Porta the functionalities of Sonix clinical software cannot be utilized.

Another implementation was developed in LabVIEW application that collected data from a dazzle (Pinnacle Systems, Mountain View, CA) and the tracking device in real-time . Both the dazzle and the tracking device were connected to a PC. US images were digitized in real-time by the dazzle. With this implementation the same kind of disadvantages were faced as Porta. The US image quality was not good enough to judge the optimal view of the carotid artery plaque.

In both of these cases, it was hard to segment the Ultrasound images; hence the plaque characteristic analysis becomes very difficult.

IV. Test and Validation Process

The position differences of sensors 2 and 4 on the forehead over two sessions were measured to understand accuracy and reproducibility of the system. The sensor 2 and 4 positions from the first session are the reference points for a follow up session. The distance (in mm) between the sensors positions on the forehead over the sessions were calculated. Reproducibility of the system is dependent on the delta of coordinate values on different sessions.

Following the intra-observer variability test instruction as described in Appendix B, there are at least two sets of coordinate values for each sensor, one set being the initial position and the other from the follow-up session. Suppose, S_1 (x_2, y_2, and $z_{2)}$ is the coordinate position of sensor 2 with respect to sensor 3 in the initial session. The follow-up session produces S_2 (x'_2, y'_2, and z'_2) point for the sensor. As sensor 3 is the reference point for both occurrences, S1 and S2 can be considered as two different points in a reference frame. So, the distance between these two points, referred to as d_1 and d_2, gives the deviation in position between sessions.

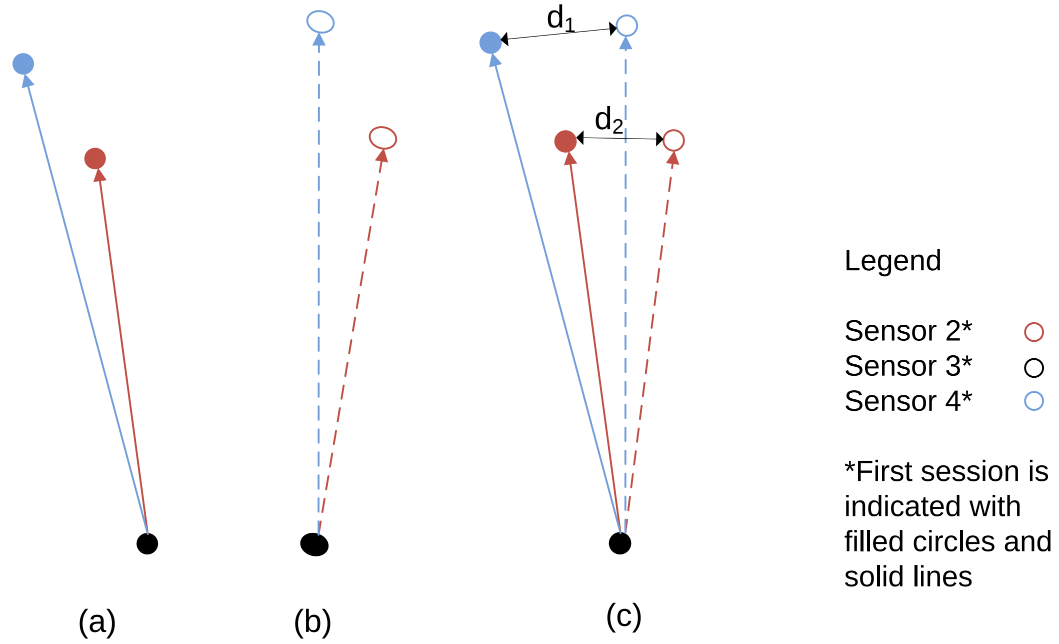

Figure 10: (a) Sensors 2 and 4 with respect to sensor 3 in the first session, (b) Sensors 2 and 4 with respect to sensor 3 in a follow-up session, (c) The first session positions superimposed on a follow-up session position. Distances (d_1 and d_2) of the first session with a follow-up session is considered to calculate precision and accuracy of the system.

The precision and accuracy of the position feedback system was measured with intra-observer variability test. The protocol for the intra-observer variability test is provided in Appendix B. Statistical mean and standard deviation were calculated to show the accuracy and precision of the system.

The position feedback system was also tested for inter-observer variability test to be confirmed that the system is not observer dependent. Different observers' performance on the position feedback system was visualized with Bland-Altman plot. The plot highlights any bias of one observer over the other.

V. Calibration

Volume reconstruction is dependent on sampling of the US image. Although the position tracking sensor attached to the ultrasound probe provides the 6-DOF position of the probe in the world coordinates, the relationship between the ultrasound image coordinate system and world coordinate system is unknown. The imaging settings, such as depth, sector angle etc affect this transformation. Calibration is performed to overcome these issues. The calibration matrix obtained in this process gives the transformation relation between the probe and the US image. In other words, calibration defines how to translate US image information into the spatial dimensions.

A string phantom was used for calibration. Two sides and the front of the phantom are made of clear plexiglass. The bottom of the phantom is also made of clear plexiglass but it has been covered with an acoustic scattering material to prevent reverberation. The rear side of the phantom is made of vinyl polymer, which allows scanning sidewise as well. The container needs to be filled with water during US scanning from the top or rear side. The side walls have been drilled to insert nylon strings of 1mm diameter. The strings are arranged to intersect each other in a plane. There are three vertical planes of strings. For the calibration, the rear most string plane was scanned from the top at various depths.

The Calibration Process

The calibration process followed for this thesis is similar in some ways to the method proposed by Pagoulatos [53]. This method is a simple and fast approach to calibration. In our approach, five readings were taken for various depths setting ranging from 3.5cm to 5.5cm in 0.5cm increment. The plane that was scanned for calibration has five strings forming six intersecting points (Figure 11). In the figure below the six points of interest are marked with letters a to f. During calibration, sensor 4 was mounted on the US probe (Figure 13).

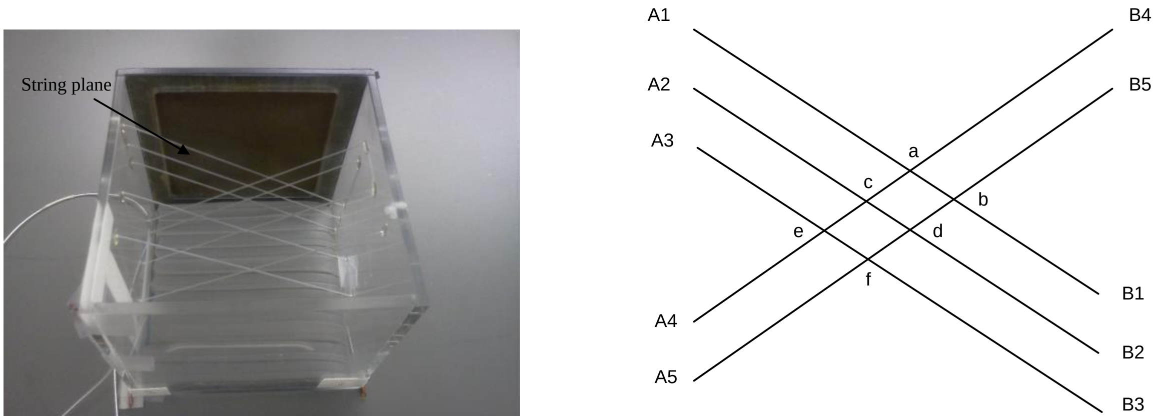

(a) (b)

Figure 11: (a) Phantom and (b) string plane

Calibration involves the four coordinate frames:

1. World coordinate frame (w): Coordinate frame is given by the transmitter.
2. Phantom coordinate frame (p): The coordinate frame that is associated with the phantom body. Sensors 1, 2 and 3 were attached to the phantom body to construct the coordinate frame (Figure 13). Sensor 3 was attached to the bottom front right corner and it was considered to be the origin of the phantom body. Sensor 2 was placed on the bottom front left corner and sensor 1 was on the top front right corner. The vector from sensors 1 to 3 is regarded as the z-axis of the phantom. Whereas, a vector from sensors 3 to 2 forms y-axis. The cross product of y- and z-axes is the x-axis.

3. Probe’s coordinate frame (s): The probe’s coordinate frame, which is actually provided by sensor 4.
4. US image coordinate frame (i): The US image is a two dimensional plane. The origin of the frame is the upper left corner. Generally, US images maintain left handed Cartesian coordinate system. In this non-standard orientation, x-axis is directed to the right and y-axis directed downwards. For the ease of calculation, this thesis kept the US coordinate system similar to other coordinate frames involved in the calibration process. Y-axis of the US image is being considered going upwards, so y coordinate values calculated from the US have negative values. Z-axis of the US image plane can be considered to be always equal to zero.

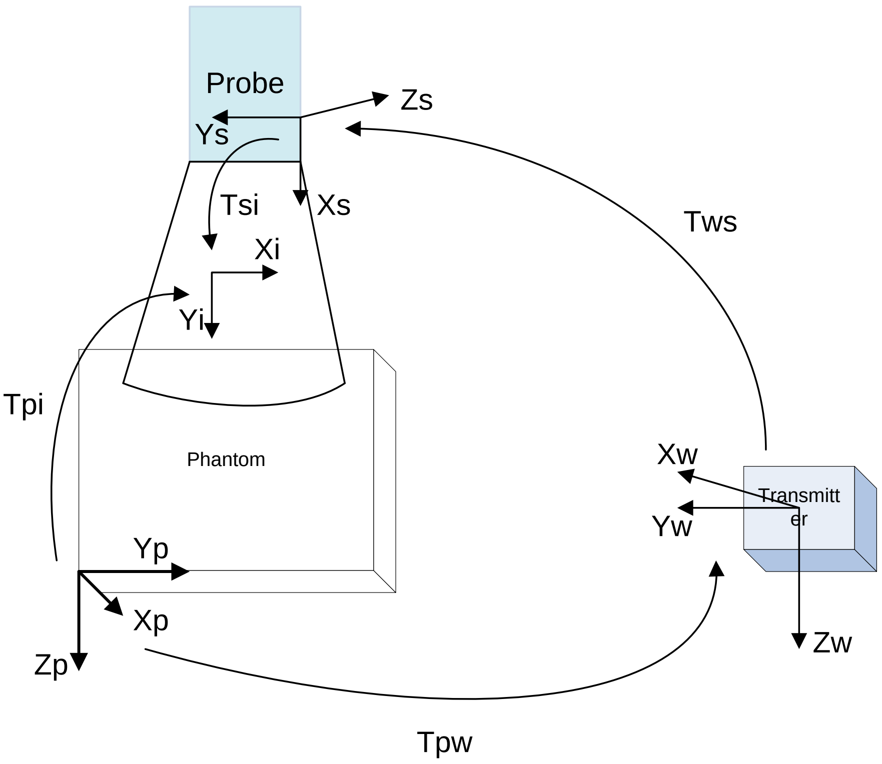

Figure 12: Coordinate frames

Figure 12 above shows the relationship between the different coordinate systems. The main purpose of the calibration process is to find the transformation between the probe and the US image (Tsi). As described by Pagoulatos, the transformation has the following relationship.

$$\mathrm{Tpi} = \mathrm{Tpw} * \mathrm{Tws} * \mathrm{Tsi} \tag{3.1}$$

$$\Rightarrow \mathrm{Tsi} = (\mathrm{Tpw} * \mathrm{Tws})^{-1} * \mathrm{Tpi} \tag{3.2}$$

The methods to find the various transformation matrices follow:

1. Transformation from the phantom to the world coordinate system (Tpw): Transformation between the transmitter (world coordinate system) and the phantom was not calculated using least square method as suggested by Pagoulatos. The transmitter is considered to be the fixed frame and the phantom is the rotated coordinate frame. Thus, the transformation from the transmitter to the phantom was found (denoted as Twp). The projection of each phantom axis onto each of the transmitter's axes were calculated to find the rotation matrix. The inverse of Twp is the asking transformation matrix, Tpw.

   Pagoulatos's method to find this matrix with Least Square Method (LSM) was not followed, because the phantom used for this thesis does not have any divots designed in it. Any six points could have been chosen to make the calculation, but that may have added to the error margin.

2. Transformation from the world coordinate system to the probe (Tws): The transformation matrix was calculated from the rotation matrix and the position coordinates retrieved from the TrakSTAR system. The rotation matrix received from the system needs to be transposed to maintain the form with other transformations.

3. Transformation from the phantom to the image coordinate system (Tpi): Least Square Method was followed to find this matrix as suggested by Pagoulatos.

The intersection points, a to f as referred in Figure 11b, were scanned. So, the image location (in form of pixel values) is known from the image. The spatial locations of the intersections were calculated with geometric equation. The end points of the line, A1-A5 and B1-B5 (Figure 11b), were measured from the outer side wall of the phantom. Line equations were found from the end points and then the intersection points between two straight lines were calculated. Even though the line slope starts from the inner side of the wall, the intersection points will remain constant as the phantom wall is uniform on all sides.

Once the three transformation matrices are found Tsi can be calculated with equation 3.2.

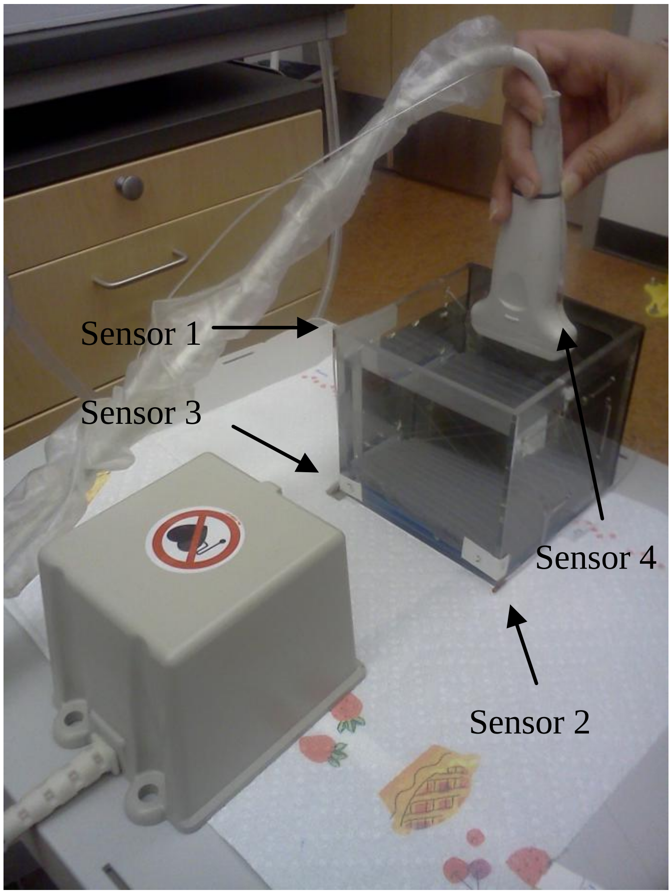

Figure 13: Calibration process.

A Matlab (The Mathworks, Incorporation, Natick, MA) program was written to detect the intersection points from the US image (Figure 14) and to calculate the calibration matrix.

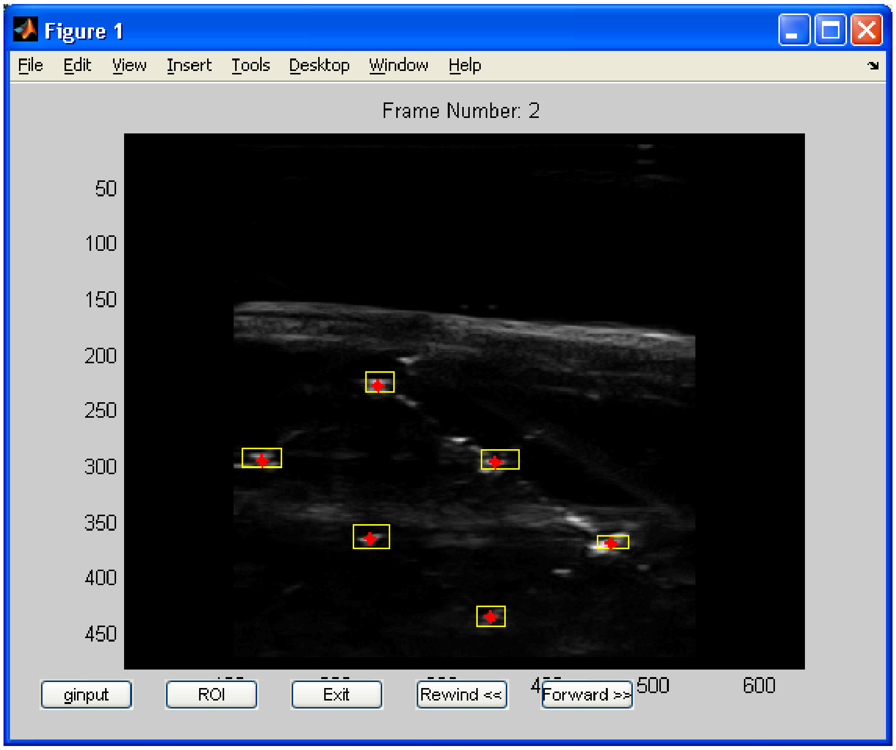

Figure 14: Detect Image points

The calibration result was reported with the mean, the standard deviation for coordinate values and the rotation matrix elements. The phantom intersection points' spatial locations were recalculated with the calibration matrix. The difference between the physical location and the calculated location gives the accuracy measurement of the process.

VI. Volume Reconstruction

Stradwin software was used to reconstruct 3D volume from freehand Ultrasound acquisition [56]. Stradwin takes the US images and associated probe coordinate values to reconstruct the volume. Sampling plays a vital role in volume reconstruction process. The freehand sweeping makes the image frames non-uniform. Frames at an angle cause volumes at a deep to have sparse samples. To solve the problem, interpolation needs to be performed on the images. Stradwin uses Cubic Mitchell-Netravali spline algorithm for interpolation.

The accuracy of the quantitative measurements of the reconstruction was calculated using a Doppler flow phantom (ATS Laboratories, Inc., Bridgeport, CT). The tissue mimicking Doppler flow phantom (523A model) contains four flow channels of 2, 4, 6, and 8mm diameters. The scanned surface of the phantom maintains 18^{o} angle with the flow channels (Figure 15).

The channel with 6mm diameter was scanned in cross sections (transverse view) and along the length (sagittal view). Scans were performed five times in each orientation at 5.5cm depth setting.

Figure 15: Doppler Phantom scanning for reconstruction

The flow channel appears as an ellipsoid structure in a cross-section US frame—more or less as a circle. 3D volume was reconstructed using Stradwin. For the reconstruction process, Stradwin requires the calibration matrix and the sensor position on the probe. The software program has a feature to put landmarks on the reconstructed volume and it can also measure the spatial distance between two pixel positions of the reconstructed volume.

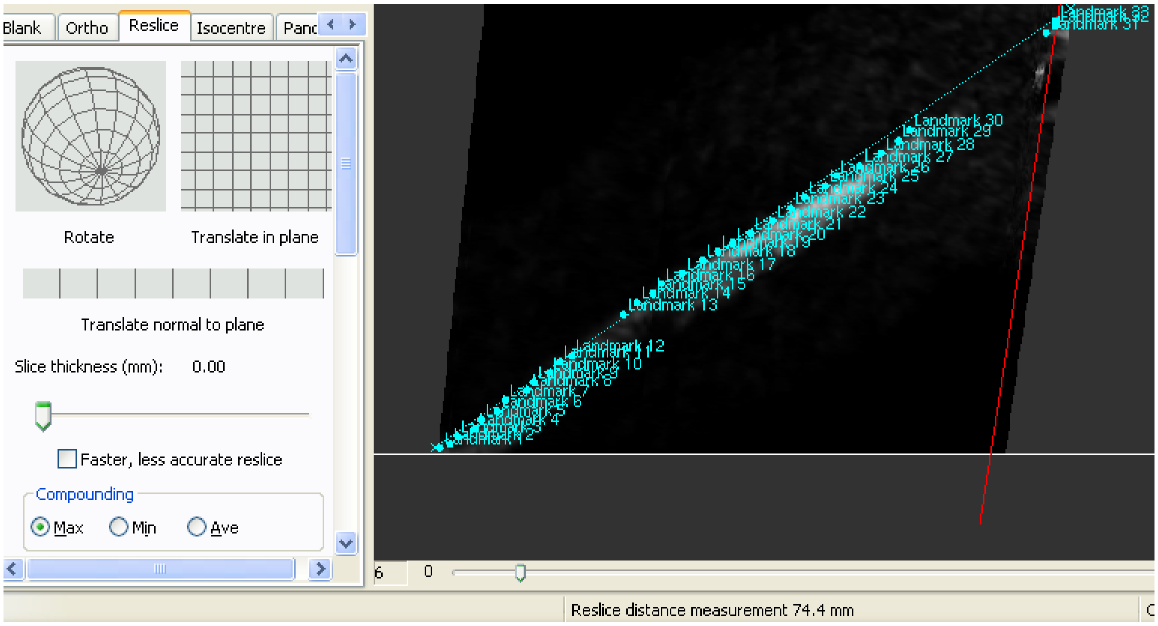

Slice thickness (mm): 0.00

☐ Faster, less accurate reslice

Compounding

● Max ○ Min ○ Ave

Reslice distance measurement 74.4 mm

Figure 16: Detecting edges with landmarks on Stradwin reconstructed volume

Several landmarks were put on the edge of the reconstructed volume (Figure 16). The landmark positions can be exported in the world coordinate system. The exported positions are expected to form a straight line. The data were analyzed with a Matlab program [64].

Chapter 4. Results and Discussion

I. Intra-Observer Variability Test

The intra-observer variability test was performed on healthy subjects with the ActiveX graphical plot display (N = 6) and raw coordinate values (N = 3) for feedback. Position reproducibility improved significantly with raw coordinate value display compared to graphical positioning feedback system ($p<0.038$). The use of sensor coordinates led to a reproducibility of (7.09+/-2.32 and 7.29+/-1.82) compared to using the graphical feedback (14.56+/-16.86 and 15.21+/-18.26), an improvement of 51% for sensor 2 and 52% for sensor 4, respectively.

During the test with the graphical positioning feedback system, few difficulties were detected by the observer. On follow-up session, per the graphical plot head position was reproduced. However data analysis revealed that the positions have diverged more than expected (Table 1). The relative distance could not be detected during the test because of the magnitude of the graphical plot axes scales. In the 3D plot, even if the markers—follow-up values and real-time values—appear to be very close, they can be more than 20mm apart, because the separation between sensors 2 and 3 (the origin of the coordinate system) is almost 300 mm.

Table 1: Position reproducibility of the system with graphical plots only

Subject ID	Sensor 2 (mm)	Sensor 4 (mm)
Subject 1	11.44	9.91
Subject 2	25.71	24.54
Subject 3	4.11	4.57
Subject 4	53.25	57.71
Subject 5	17.52	21.28
Subject 6	4.47	3.64
Mean	**14.56**	**15.21**
Std. Deviation	**16.86**	**18.26**

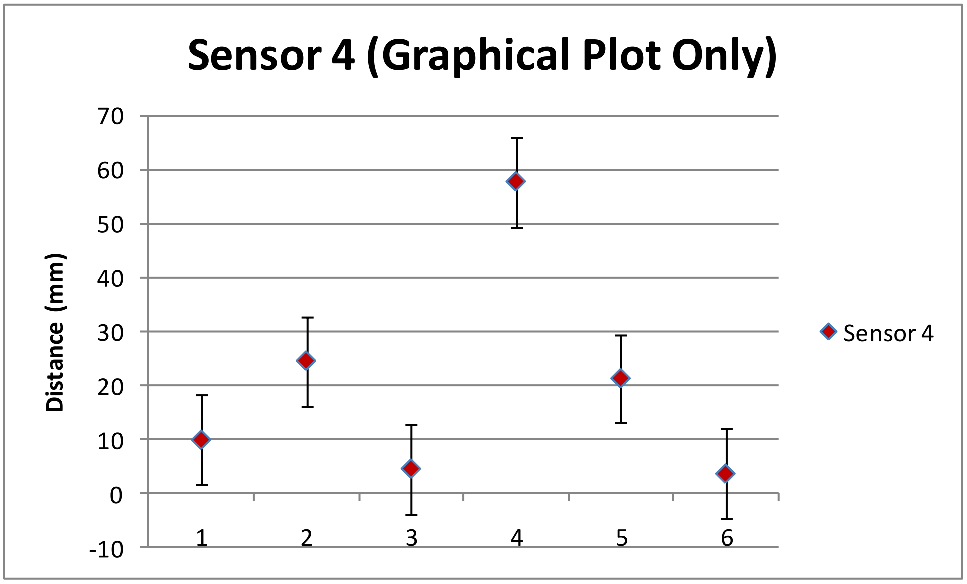

(a)

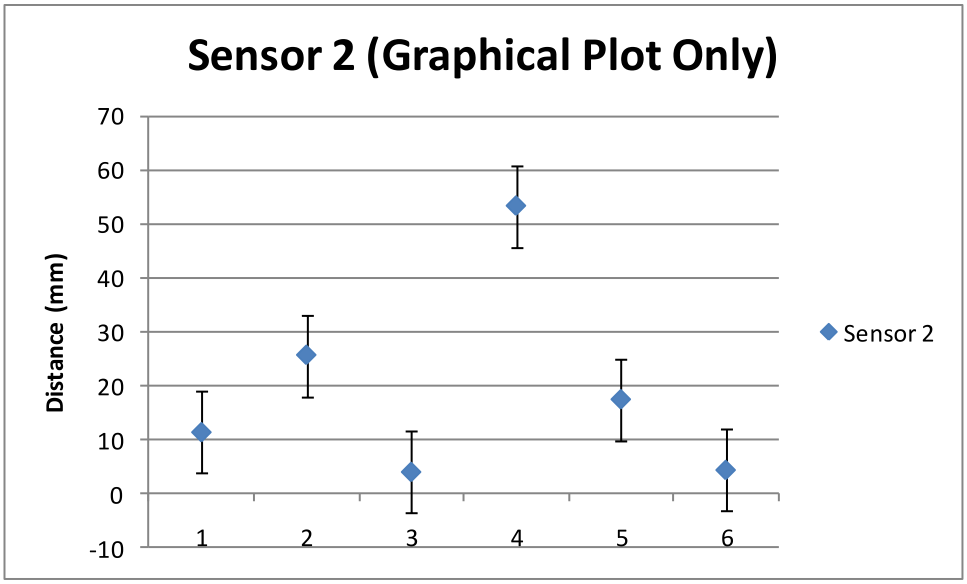

(b)

Figure 17: Position repeatability precision was measured for the system with graphical plots only with standard deviation

One possible solution was to have separate plots for the sensors on the forehead. In this way a closer look could have been achieved. The downside of this solution is that the number of plots; hence objects for the observer to handle, increases. To be able to make sure the markers have interpolated, the 3D graph needed to be rotated and viewed from different directions. Separating the plots would require manipulating two plots, which could be very difficult for the observer.

In the second approach with the coordinate value display, intra-observer variability test was performed on three healthy subjects. It was apparent during the test that the observer felt confident about accuracy of reproducibility and the process took much less time. As mentioned above, in this method the accuracy increased 51% and 52% for sensor 2 and sensor 4 respectively.

Table 2: Position reproducibility of the system with graphical plots and coordinate values

Subject	Sensor 2 (mm)	Sensor 4 (mm)
Subject 1	7.15	7.29
Subject 2	4.22	5.06
Subject 4	9.9	9.52
Mean	**7.09**	**7.29**
Std. Deviation	**2.32**	**1.82**

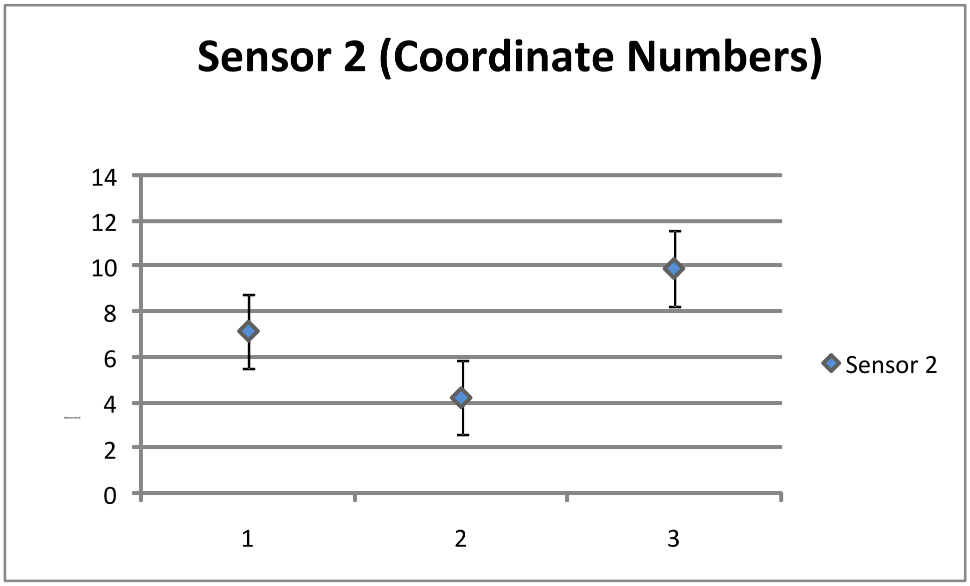

(a)

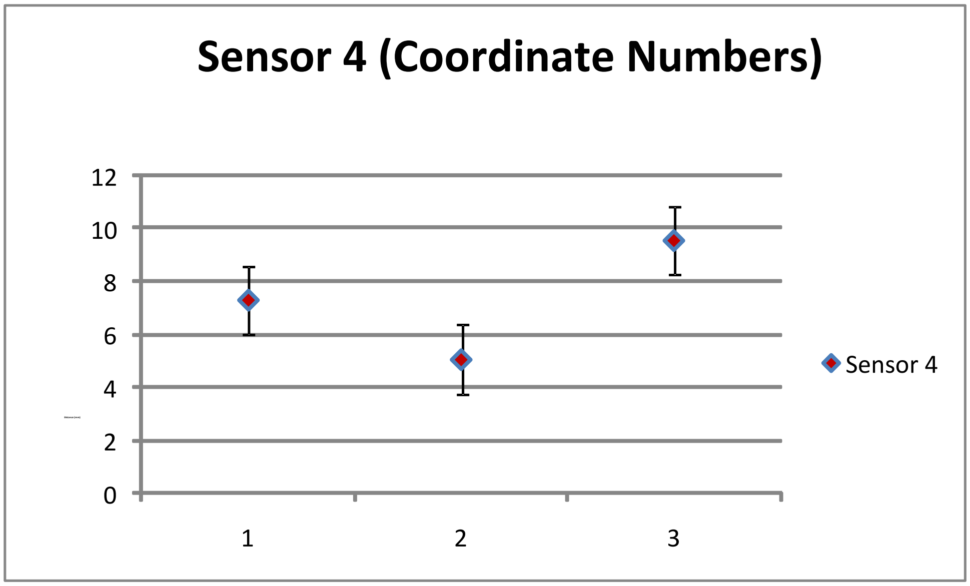

(b)

Figure 18: Position repeatability precision was measured for the system with coordinate values displayed with standard deviation

The system can reproduce the sensor position within 1cm distance. The measurement was taken with respect to sensor 3, which is almost 28cm away from the sensors on the forehead. The carotid artery bifurcation is typically about 10cm away from manubrium. A 0.7cm deviation at the forehead will cause around (0.7*10)/28 = 0.25cm displacement at carotid artery. It is unknown that how the carotid artery geometry will be affected by a 0.25cm of displacement. Further studies can be performed with this system to monitor the carotid artery geometry.

The performance of the system can be further improved. Instead of placing two sensors, only one sensor with its axes can be displayed. In this way, the observer may concentrate on only one viewing object, instead of two (sensor 2 and 4). Both the graphical and raw coordinate values can be used for fine tuning the patient position, then the US frame rate should be much less so that not a significant amount is lost. Lost frames will affect the volume reconstruction process.

II. Inter-Observer Variability Test

The inter-observer variability test was performed on two healthy subjects by two observers. Bland-Altman plots show that all of the data are within the range of 95% confidence interval (CI).

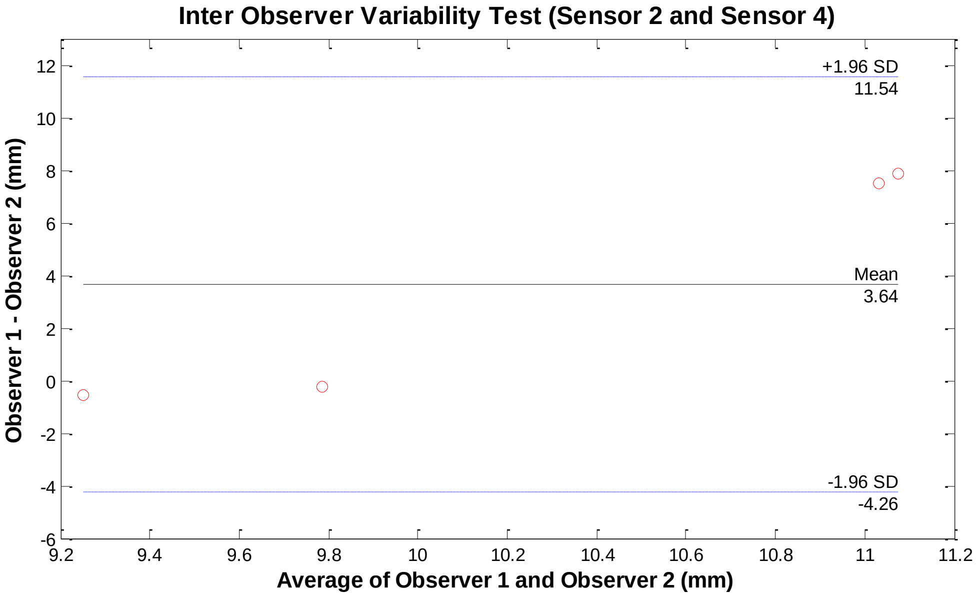

Figure 19: Inter-Observer Variability Test for Sensor 2 and Sensor 4 was analyzed with Bland-Altman Plot for the system with graphical plots and coordinate value displays

Only two subjects is a very small sample size to make any decision. Further tests should be performed to make a better conclusion regarding the inter-observer variability on the system.

III. Calibration

Calibration was performed for 3.5cm to 5.5cm depth in 0.5cm increment. At each depth five images were acquired. The mean, standard deviation, and standard error were reported for each depth separately (Table 3). The positions of the transformation matrix and the first two columns of the rotation matrix are shown in the table below. The third column of the rotation matrix is just the cross product of the first two columns. A smaller number in the standard deviation column indicates that the calibration matrix is stable.

Table 3: Calibration result for 35mm, 40mm, 45mm, 50mm, and 55mm

		X(mm)	Y(mm)	Z(mm)	R11	R21	R31	R12	R22	R32
35mm	Mean	36.97	-4.27	2.61	-0.044	0.751	0.655	-1.000	-0.060	-0.031
	Std. Dev	1.02	1.56	0.64	0.007	0.006	0.007	0.001	0.007	0.008
40mm	Mean	37.07	-8.13	0.42	-0.036	0.741	0.667	-1.001	-0.062	-0.022
	Std. Dev	1.31	0.64	0.50	0.007	0.004	0.005	0.001	0.003	0.003
45mm	Mean	37.78	-13.33	-3.20	-0.038	0.795	0.586	-1.000	-0.068	-0.011
	Std. Dev	0.36	4.07	5.31	0.003	0.079	0.123	0.001	0.007	0.018
50mm	Mean	37.32	-15.92	-0.63	-0.042	0.757	0.644	-1.000	-0.064	-0.023
	Std. Dev	0.63	5.56	8.88	0.004	0.052	0.069	0.000	0.007	0.009
55mm	Mean	37.15	-12.50	-7.05	-0.039	0.713	0.695	-1.000	-0.058	-0.029
	Std. Dev	0.98	8.77	0.57	0.004	0.038	0.036	0.000	0.004	0.005

The calibration matrix is much stable at a lower depth setting. At each depth setting error in reconstructing from the image depth were calculated.

Table 4: Difference between calculated point location and spatial location at different depth of an image for different depth settings

Phantom Points*	35mm	40mm	45mm	50mm	55mm
a	0.83	0.84	0.87	0.85	0.81
b	1.32	1.26	1.25	1.30	1.38
c	0.44	0.42	0.45	0.44	0.48
d	0.47	0.49	0.50	0.53	0.51
e	1.48	1.49	1.48	1.56	1.53
f	0.71	0.67	0.68	0.68	0.69

*Refer to Figure 11b.

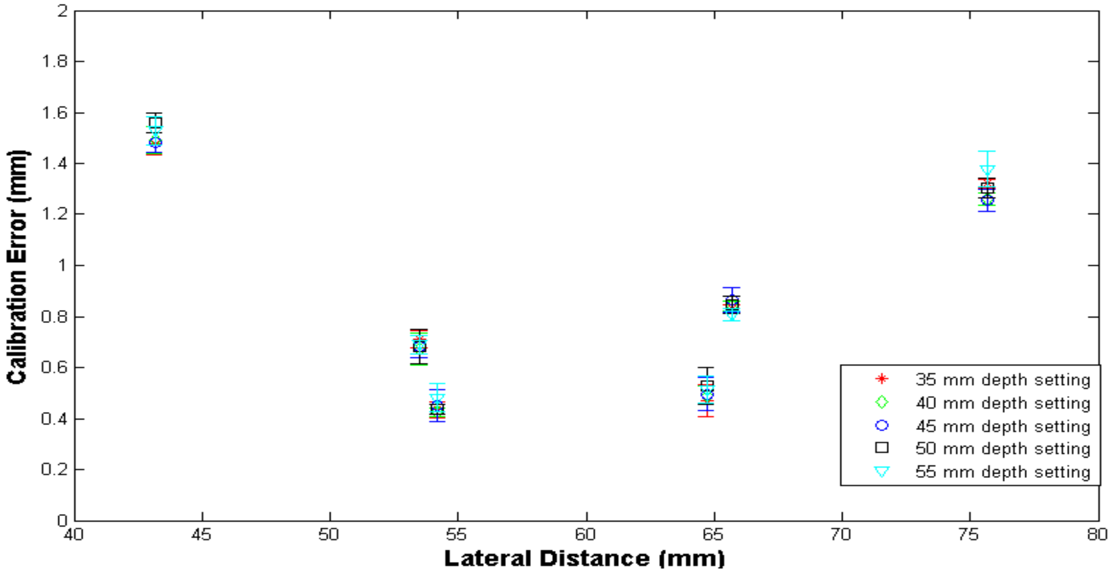

Figure 20: Comparing calibration error due to Ultrasound machine depth settings

The accuracy of the calibration matrix can be tested by comparing a known spatial point location with the one computed using the calibration matrix. The six points were recalculated using the calibration matrix and were matched with the known location points. The difference accuracy of the calibration matrix is tabulated in Table 5.

Table 5: Relative accuracy of the calibration matrix

	35mm	40mm	45mm	50mm	55mm
Mean (mm)	1.39	1.36	1.37	1.42	1.43
Std. Dev. (mm)	0.02	0.01	0.03	0.03	0.03

Theoretically, calibration matrix should be identical for each reading at a certain depth. The difference occurs because the probe may not be scanning at the exact plane of the strings. Still, the six points are picked up by the US machine, because both the probe beam and the strings have a finite width. The calibration matrix is also affected by the accuracy of locating the intersection points from the US image (Figure 14). The brightest pixel in a selected region for an intersection may not be the center of the intersection.

IV. Volume Reconstruction

The landmark positions from the edge of the reconstructed phantom volume were plotted in Matlab and a straight line was fitted through the points (Figure 16). The landmark positions can be exported in the world coordinate system. The exported positions are expected to form a straight line. Figure 21 shows one set of data that fits a straight line through the landmark positions with the average approximation error of 0.006mm and the maximum error is 0.09mm.

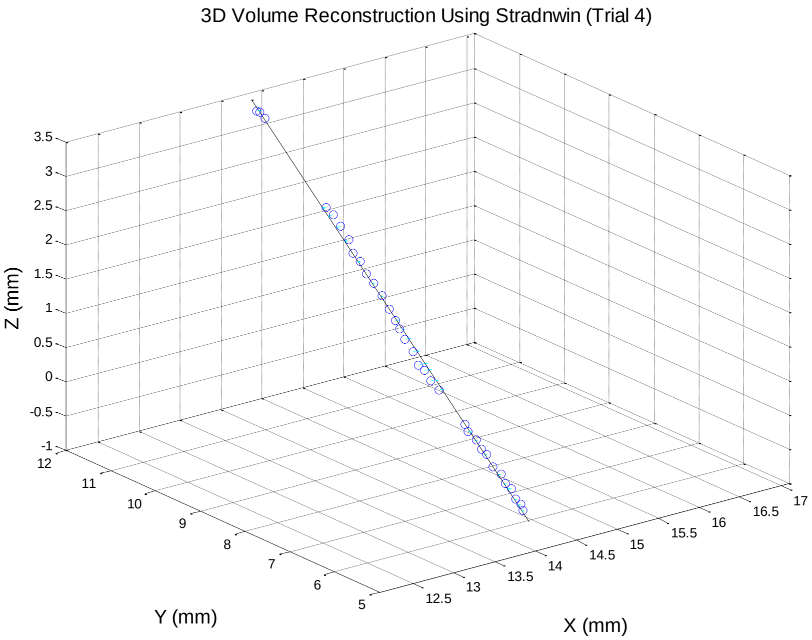

Figure 21: Edge detection precision of the reconstructed phantom volume

The error is due to the manual segmentation of the volume.

Chapter 5. Conclusion

This thesis developed a system to enable reproducibility in freehand US grayscale image for a longitudinal study. US grayscale imaging is sensitive to the insonation angle. The insonation angle depends on the US probe's position relative to the anatomy and the neck position. Both the features need to be reproducible in order to compare US images for a longitudinal study. A software application was developed as a part of this thesis, which guides a patient to reproduce the head position using a magnetic tracking device. The system also tracks the probe's position and orientation in real time that enables the reconstruction of a 3D volume out of the grayscale images. Calibration was performed using a custom-built string phantom. The precision and the accuracy of the calibration method were reported with mean, standard deviation and standard error numbers.

With intra- and inter-observer variability tests, it has been found that the patients' head position can be reproduced with an average error of 7 mm. The images acquired with freehand US grayscale were reconstructed for 3D volume using Stradwin. The volume quality can be improved by correcting probe pressure factor and integrating EKG gating into the system for tracking cardiac cycle variability.

The software system can be used for further studying the carotid artery geometry. However, its use does not have to be limited to the study of the carotid artery only. Any longitudinal anatomical scan of any variable length that may require real-time position or orientation data acquisition may use the system.

Appendix A. Acquiring Freehand US Data with 3D Guidance TrakSTAR

1. Patient lying in supine position.
2. Place the transmitter on the bed with the front side facing the patient and make sure the tracking device electronic unit is up and running.
3. Sensor 1 will be attached to the probe.
4. Place sensors on the patient.

a. Sensors 2 and 4 are places on the forehead in a line. Tip of the sensor 2 should be in between eyebrows aligned with the upper line of the brows (figure 1). Sensors should be fixed on a rigid body (a piece of plastic or wooden piece that does not bend).

Figure 22: Sensor 2 and sensor 4 are attached to a rigid body. The rigid body is place on the forehead of the patient such that the tip of sensor 2 is in between the eyebrows

b. Sensor 3 should be on the manubrium pointing towards the head of the patient (figure 2).

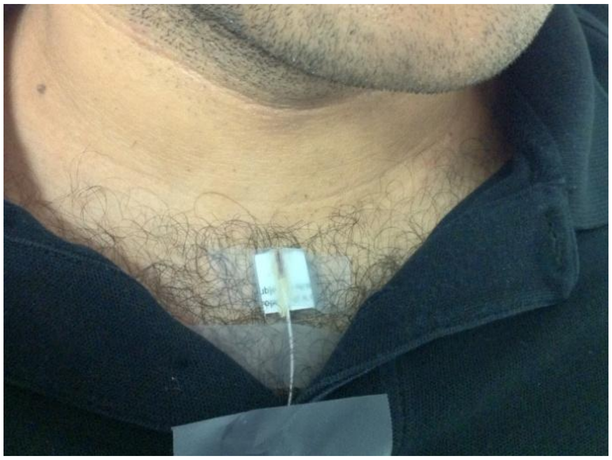

Figure 23: Sensor 3 is placed on the manubrium

5. Open SONIX program, press Q button, choose Vascular preset from the exam application, choose L14-5/38 as scanning transducer, insert patient ID.
6. Set Frame per Second (FPS) parameter to 13Hz or less by increasing the focus number.
7. Open the Ulterius application and insert patient ID and IP address in the ‘Server Name’ field and then hit connect (figure 4). In case Ulterius is running on the Ultrasound machine, IP address should be ‘127.0.0.1’.

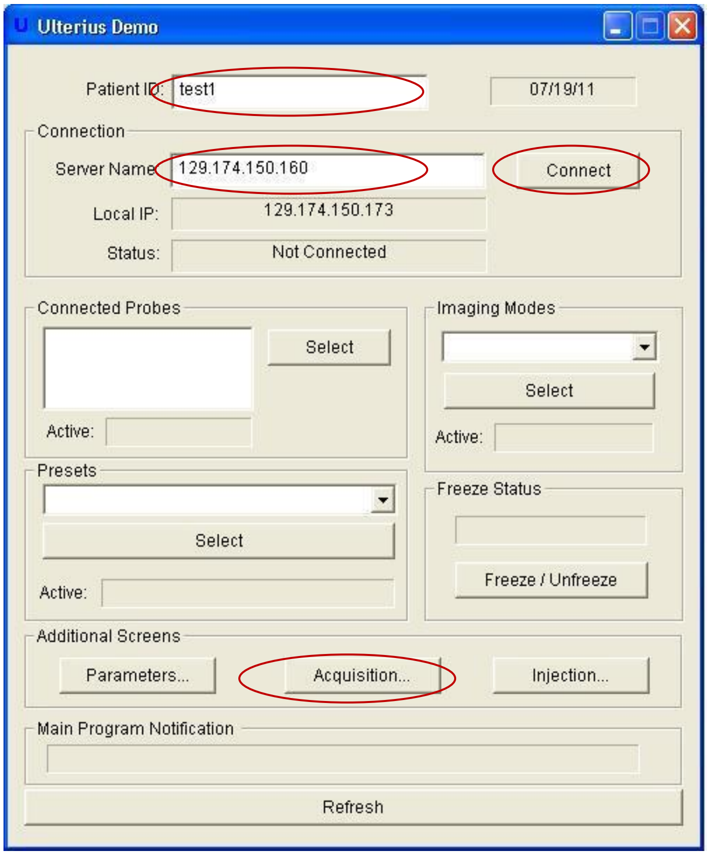

Patient ID: test1

07/19/11

Server Name: 129.174.150.160

Local IP: 129.174.150.173

Status: Not Connected

Figure 24: Main window for Ulterius

After connecting to the Sonix software, Ulterius creates a new window displaying position data (figure 5). The ‘connect’ button toggles to ‘disconnect’.

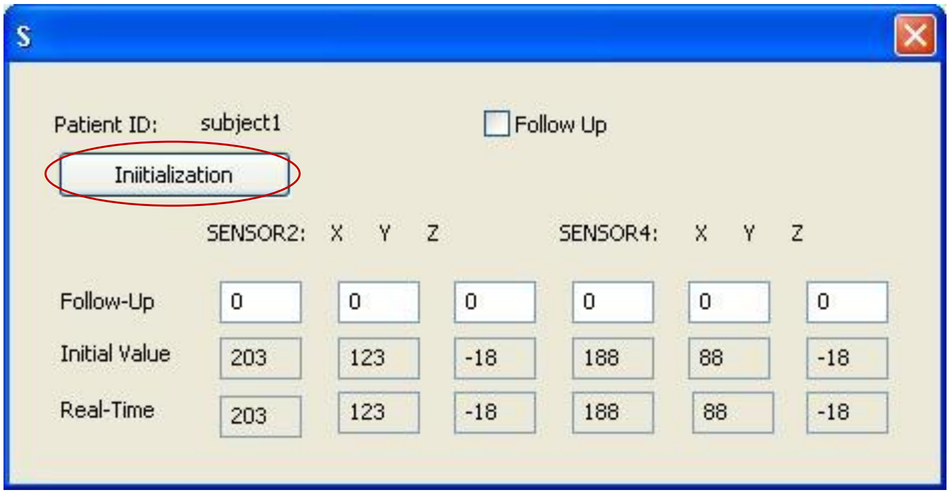

Patient ID: subject1

☐ Follow Up

	SENSOR2: X	Y	Z	SENSOR4: X	Y	Z
Follow-Up	0	0	0	0	0	0
Initial Value	203	123	-18	188	88	-18
Real-Time	203	123	-18	188	88	-18

Figure 25: Position feedback system window

8. Press “Acquisition” button on the Ulterius graphical user interface (GUI) (figure 3) which will create a new window (figure 5). This window takes user input for the type of US data it should store.

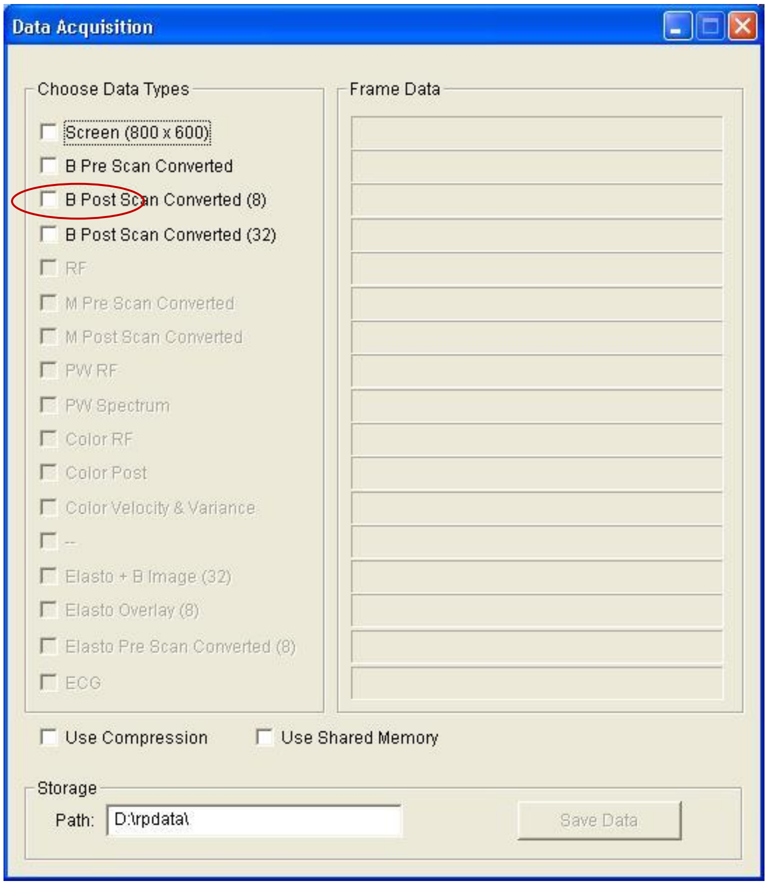
Data Acquisition

Choose Data Types

☐ Screen (800 x 600)
☐ B Pre Scan Converted
☐ B Post Scan Converted (8)
☐ B Post Scan Converted (32)
☐ RF
☐ M Pre Scan Converted
☐ M Post Scan Converted
☐ PW RF
☐ PW Spectrum
☐ Color RF
☐ Color Post
☐ Color Velocity & Variance
☐ --
☐ Elasto + B Image (32)
☐ Elasto Overlay (8)
☐ Elasto Pre Scan Converted (8)
☐ ECG

Frame Data

☐ Use Compression ☐ Use Shared Memory

Storage

Path: D:\rpdata\

Save Data

Figure 26: Data acquisition window

9. Have the patient lying down with face straight up, press ‘Initialization’ button (figure 4). This step will record the normal lying position of the patient.
10. Scan the carotid artery in transverse or sagittal plane to get an understanding of the artery geometry.
11. Once the sonographer is satisfied with the head position and quality of image, freeze scanning. The patient should maintain the head rotation.
12. Check the type of data needs to be recorded in Acquisition window (figure 5).
13. Hit Unfreeze button and scan the artery back and forth once.
14. Take a snapshot (‘print 1’ button).
15. Disconnect Ulterius. The ‘Disconnect’ button is the same as the connecting button from the main window (figure 3). **If the Ulterius needs to be reconnected, please change the patient ID first, else the output result will be overwritten.**

16. Collect the following output files from D://rpdata folder: ‘Patient ID’.csv and ‘Patient ID’_params.txt. Suppose, the patient ID was ‘test1’, then the two generated files will be test1.csv and test1_params.txt.

Appendix B. Intra-observer Variability Test

1. For the initial visit follow the instructions provided on Appendix A. Rather than using a sweep on the artery, a snapshot of the optimal view of the artery is used as this is sufficient for this test.
2. Make a note of the positions from the saved .csv file.
3. Take off the sensors from the patient. The follow up session can be performed at any later time.
4. For a follow-up session the procedure is same, except the follow up information needs to be added to the fields (Figure 25) and instead of positioning arbitrarily the head should be matched with the previous head position and orientation.

Appendix C. Custom Software Operation Flow

The custom software (Ulterius) operation maintains the following states (Figure 27): Start-up, Initial Position, Data Collection, Wait, and Halt.

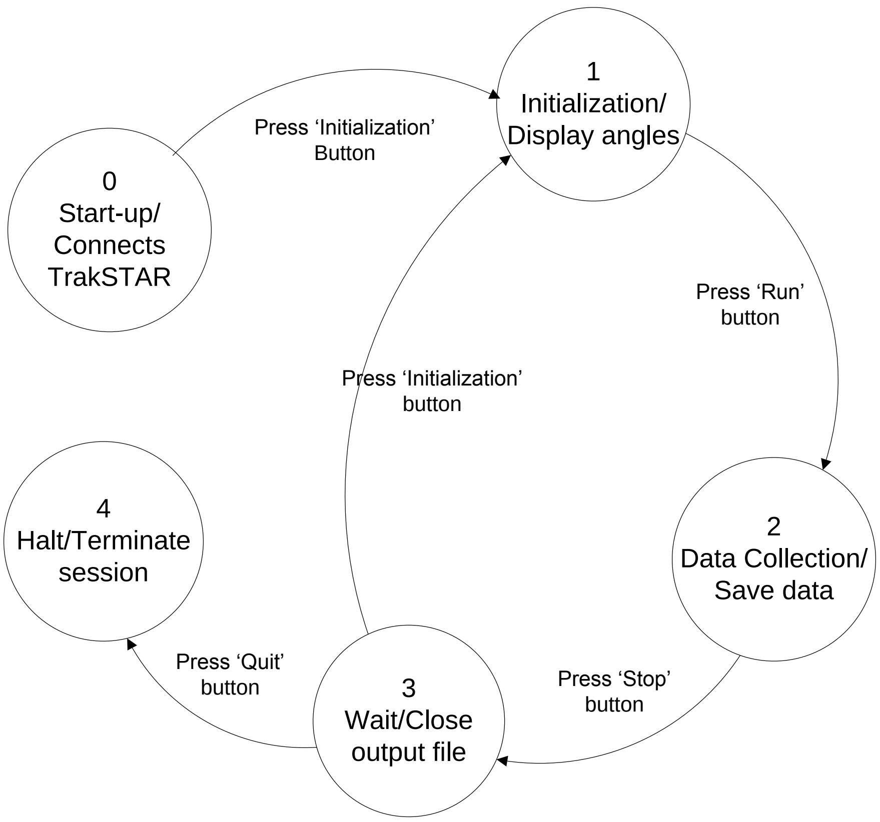

Figure 27: Custom developed software Finite State Machine (FSM)

State 0 (Start-up): This is the start-up state that starts with the application and connects to the modalities (trakSTAR and US machine).

State 1 (Initial Position): In this state the head position is displayed either in terms of angle or position. No data is stored in this state of the system; rather the sonographer is responsible of finding the best image of the carotid artery plaque. The sonographer may ask the patient to reposition their head to find the best image.

State 2 (Data Collection): Once the sonographer is satisfied with the quality of the stenosis image, he/she may start collecting the data. The system stores US frame data and trakSTAR one after another. In this way a US images can be tagged with the associated positioning information using frame ordering or timestamp.

State 3 (Wait): Data collection can be stopped. The sonographer may start a fresh batch of scanning with different head positions which takes the system to State 1 or may run in the same settings to get another set of data which leads the system to State 2;

State 4 (Halt): The system also has an option to exit from any state. Before exiting the system, all connections are closed.

Appendix D. The Pose of a Sensor with Respect to Another Sensor

The position feedback system displays sensor 2 and 4 position in respect to sensor 3. The change in a sensor's reference frame is performed by the system itself. The method to pose a sensor respect to another sensor is provided below:

1. Ascension 3D Guidance provides several types of data for each sensor. Choose a data type that provides at the position coordinates (x, y, and z values) and the rotation matrix (3x3 matrix). Suppose, sensor 2 should be posed in sensor 3 coordinate system (Figure 28).

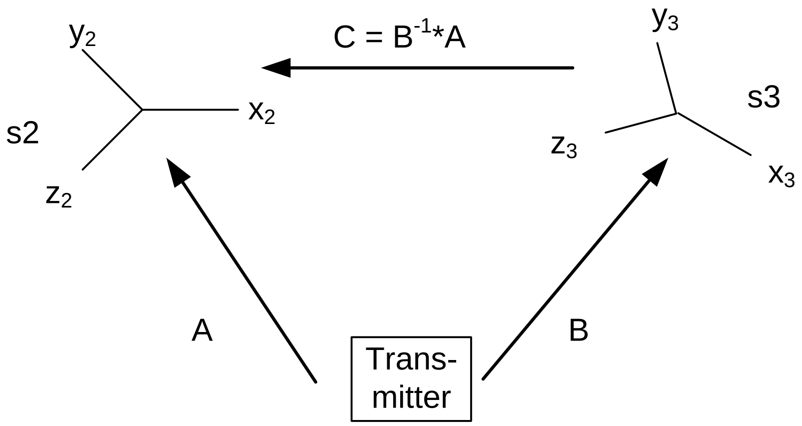

Figure 28: Changing coordinate frame of a sensor

2. A and B are the 4x4 transformation matrices in Figure 28 for sensor sensors 2 and 4, respectively. Transformation matrices are built from the rotation and the translation matrices. Suppose, the rotation matrix received from the Ascension device is,

$$\mathrm{R} = \begin{bmatrix} \mathrm{r11} & \mathrm{r12} & \mathrm{r13} \\ \mathrm{r21} & \mathrm{r22} & \mathrm{r23} \\ \mathrm{r31} & \mathrm{r32} & \mathrm{r33} \end{bmatrix}$$

The rotation matrix, using Euler angle notation, returned from the system has the following form.

$$\begin{matrix} \mathrm{CE} * \mathrm{CA} & \mathrm{CE} * \mathrm{SA} & -\mathrm{SE} \\ -(\mathrm{CR} * \mathrm{SA}) + (\mathrm{CR} * \mathrm{SE} * \mathrm{CA}) & (\mathrm{CR} * \mathrm{CA}) + (\mathrm{CR} * \mathrm{SE} * \mathrm{SA}) & \mathrm{CR} * \mathrm{CE} \\ (\mathrm{CR} * \mathrm{SA}) + (\mathrm{CR} * \mathrm{SE} * \mathrm{CA}) & -(\mathrm{CR} * \mathrm{CA}) + (\mathrm{CR} * \mathrm{SE} * \mathrm{SA}) & \mathrm{CR} * \mathrm{CE} \end{matrix}$$

Where, CE = COS(E), CA = COS(A), CR = COS(R), SE = SIN(E), and SA = SIN(A)

If the position of a sensor is Tr = $\begin{bmatrix} x \\ y \\ z \end{bmatrix}$, then the transformation matrix is as follows,

$$\mathrm{Tf} = \mathrm{Tr} * \mathrm{R}^{\mathrm{T}}$$

$$\Rightarrow \text{Tf} = \begin{bmatrix} 1 & 0 & 0 & x \\ 0 & 1 & 0 & y \\ 0 & 0 & 1 & z \\ 0 & 0 & 0 & 1 \end{bmatrix} * \begin{bmatrix} \text{r11} & \text{r12} & \text{r13} & 0 \\ \text{r21} & \text{r22} & \text{r23} & 0 \\ \text{r31} & \text{r32} & \text{r33} & 0 \\ 0 & 0 & 0 & 1 \end{bmatrix}$$

3. As shown in Figure 28 above, the inverse of B needs to be computed. From the properties of transformation matrix, the inverse can be computed as

   $$\text{Tf}^{-1} = \text{R}^{-1} * \text{Tr}^{-1}$$

   $$\Rightarrow \text{Tf} = \begin{bmatrix} \text{r11} & \text{r21} & \text{r31} & 0 \\ \text{r12} & \text{r22} & \text{r32} & 0 \\ \text{r13} & \text{r23} & \text{r33} & 0 \\ 0 & 0 & 0 & 1 \end{bmatrix} * \begin{bmatrix} 1 & 0 & 0 & -x \\ 0 & 1 & 0 & -y \\ 0 & 0 & 1 & -z \\ 0 & 0 & 0 & 1 \end{bmatrix}$$

   A rotation matrix retrieved from the TrakSTAR system can be directly used in finding the inverse of a transformation matrix. The rotation matrix need not be transposed twice, first to create a transform matrix and then to find the inverse of the rotation matrix.

4. Multiplying the transformation and the inverse transformation matrices, respectively of sensors 2 and 3, will produce the desired transformation matrix that puts sensor 2 in sensor 3’s coordinate system. The last column of the calculated matrix gives the position and first 3x3 elements gives the rotational matrix. However, the rotational matrix needs to be transposed to have it in a similar form as the device.

Appendix E. Software Design

The system was developed in Visual Studio 2010 (Microsoft Corporation) environment. It was built on Ulterius Graphical User Interface (GUI) demo program provided by Ultrasonix. Ulterius is a Software Development Kit (SDK) that allows users to control the Ultrasonic machine remotely. However, Ulterius was used on the same machine. But the SDK was chosen because it connects to Sonix MDP clinical software and can utilize presets for carotid artery imaging. The SDK also supports real-time data collection, hardware control for Time-Gain Compensation (TGC), device synchronization through software interrupts, transducer selection capabilities, and different imaging modes. The demo code was modified to integrate trakSTAR Application Programming Interfaces (APIs).

The application was designed into several modules (classes) to distribute responsibilities. The ‘CMainDlg’ class is the hub of the program. It creates channel with US data stream and the tracking device. This class also synchronizes image frame with positioning data. ‘CMainDlg’ spawns ‘CAcquireDlg’ and ‘CPlotDlg’ class objects. ‘CAcquireDlg’ is responsible for storing image data in a file. Whereas, ‘CPlotDlg’ creates position feedback system of the probe and subject’s head position and stores the data in a file.

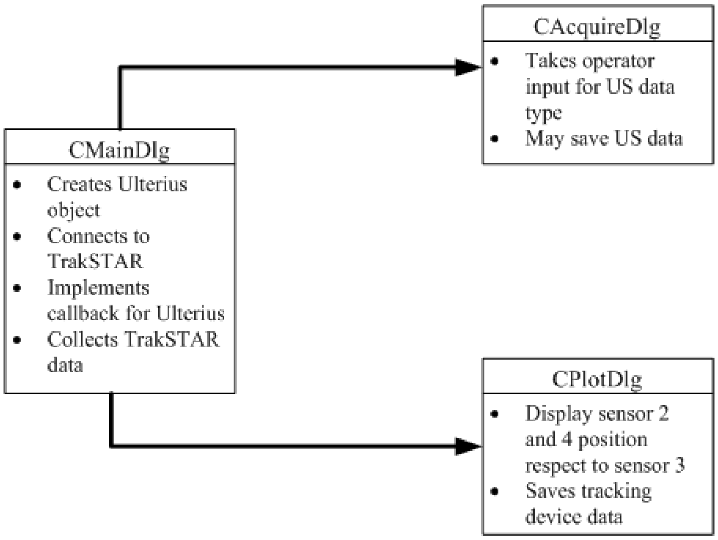

Figure 29: Software Design

The position feedback system allows the sonographer detect any movement on the patient head position. Also, for a follow-up session the feedback system shows previous positions and the real-time positions. Thus, the primary aim of this project to reproduce the angle insonation is achieved using the system. The sensor coordinate positions on the forehead (sensor 2 and 4) and the probe (sensor 1) are always recalculated in reference to sensor 3 at the manubrium. Appendix D includes methods to pose a sensor position with respect to another sensor instead of the transmitter.

The synchronization of the US frame and positioning data happens in ‘CMainDlg’ class method using Ulterius' callback functionality. Upon a frame availability, Ulterius calls a callback function. Parameters of the callback function specify frame number and data. Within the callback function a new thread is created to pass the image data onto

‘CAcquireDlg’ class method, read tracking device data for all sensors, and pass them to 'CPlotDlg' class method.

Since the tracking device data is being accessed only when a US image frame is available, it can be safely concluded that the two data are synchronized.

References

References

[1] C.P. Allott, C.D. Barry, R. Pickford, and J.C. Waterton, “Volumetric assessment of carotid artery bifurcation using freehand-acquired, compound 3D ultrasound,” *The British Journal of Radiology*, vol. 72, Mar. 1999, pp. 289-292.

[2] N. Aristokleous, I. Seimenis, Y. Papaharilaou, G. Georgiou, B. Brott, E. Eracleous, and A. Anayiotos, “Effect of Posture Change on the Geometric Features of the Healthy Carotid Bifurcation,” *IEEE TRANSACTIONS ON INFORMATION TECHNOLOGY IN BIOMEDICINE*, vol. 15, 2011, pp. 148-154.

[3] H. Tang, R.S. van Onkelen, T. van Walsum, R. Hameeteman, M. Schaap, F.L. Tori, Q.J.A. van den Bouwhuijsen, J.C.M. Witteman, A. van der Lugt, L.J. van Vliet, and W.J. Niessen, “A semi-automatic method for segmentation of the carotid bifurcation and bifurcation angle quantification on black blood MRA,” *Medical Image Computing and Computer-Assisted Intervention: MICCAI ... International Conference on Medical Image Computing and Computer-Assisted Intervention*, vol. 13, 2010, pp. 97-104.

[4] A. Fenster, C. Blake, I. Gyacskov, A. Landry, and J.D. Spence, “3D ultrasound analysis of carotid plaque volume and surface morphology,” *Ultrasonics*, vol. 44, Dec. 2006, p. e153-e157.

[5] F.P. Glor, B. Ariff, A.D. Hughes, P.R. Verdonck, D.C. Barratt, A.D. Augst, S.A.M. Thom, and X.Y. Xu, “Influence of head position on carotid hemodynamics in young adults,” *American Journal of Physiology. Heart and Circulatory Physiology*, vol. 287, Oct. 2004, pp. H1670-1681.

[6] A. Delcker and H.C. Diener, “3D ultrasound measurement of atherosclerotic plaque volume in carotid arteries,” *Bildgebung = Imaging*, vol. 61, Jun. 1994, pp. 116-121.

[7] A. Delcker and H.C. Diener, “Quantification of atherosclerotic plaques in carotid arteries by three-dimensional ultrasound,” *Br J Radiol*, vol. 67, Jul. 1994, pp. 672-678.

[8] A. Fenster, D. B. Downey, and H. N. Cardinal, “Three-dimensional ultrasound imaging,” *Physics in Medicine and Biology,* vol. 46, no. 5, p. R67-R99, 2001.

[9] A. Gee, R. Prager, G. Treece, and L. Berman, “Engineering a freehand 3D ultrasound system,” *Pattern Recognition Letters*, vol. 24, Feb. 2003, p. 757–777.

[10] M. Gerhard-Herman, J.M. Gardin, M. Jaff, E. Mohler, M. Roman, and T.Z. Naqvi, “Guidelines for noninvasive vascular laboratory testing: a report from the American Society of Echocardiography and the Society of Vascular Medicine and Biology,” *Journal of the American Society of Echocardiography: Official Publication of the American Society of Echocardiography,* vol. 19, Aug. 2006, pp. 955-972.

[11] Q.H. Huang, Y.P. Zheng, M.H. Lu, and Z.R. Chi, “Development of a portable 3D ultrasound imaging system for musculoskeletal tissues,” *Ultrasonics*, vol. 43, 2005, pp. 153-163.

[12] A. Landry, J.D. Spence, and A. Fenster, “Measurement of Carotid Plaque Volume by 3-Dimensional Ultrasound,” *Stroke*, vol. 35, Apr. 2004, pp. 864-869.

[13] M. Lécart, M.-H.R. Cardinal, Z. Qin, G. Soulez, and G. Cloutier, “In vitro in-stent restenoses evaluated by 3D ultrasound,” *Medical Physics*, vol. 36, 2009, p. 513.

[14] U. Schminke, L. Motsch, L. Hilker, and C. Kessler, “Three-Dimensional Ultrasound Observation of Carotid Artery Plaque Ulceration,” *Stroke*, vol. 31, Jul. 2000, pp. 1651-1655.

[15] N. Thune, O.H. Gilja, T. Hausken, and K. Matre, “A practical method for estimating enclosed volumes using 3D ultrasound,” *European Journal of Ultrasound*, vol. 3, 1996, pp. 83-92.

[16] B. Yip and J.S. Jin, “Pose determination and viewpoint determination of human head in video conferencing based on head movement,” *Multimedia Modelling Conference, 2004. Proceedings. 10th International*, 2004, pp. 130-135.

[17] M.L. Bots, A.W. Hoes, P.J. Koudstaal, A. Hofman, and D.E. Grobbee, “Common Carotid Intima-Media Thickness and Risk of Stroke and Myocardial Infarction : The Rotterdam Study,” *Circulation*, vol. 96, Sep. 1997, pp. 1432-1437.

[18] J. Boisvert, D Gobbi, S Vikal, R Rohling, G Fichtinger, P Abolmaesumi, “An Open-Source Solution for Interactive Acquisition, Processing and Transfer of Interventional Ultrasound Images”, MICCAI 2008.

[19] A.C. Bovik, “On detecting edges in speckle imagery,” Acoustics, Speech and Signal Processing, IEEE Transactions on, vol. 36, 1988, pp. 1618-1627.

[20] R.O. Duda and P.E. Hart, “Use of the Hough transformation to detect lines and curves in pictures,” Communications of the ACM, vol. 15, 1972, p. 11–15.

[21] R.N. Czerwinski, D.L. Jones, and W.D. O’Brien, “An approach to boundary detection in ultrasound imaging,” Ultrasonics Symposium, 1993. Proceedings., IEEE 1993, 1993, pp. 951-955 vol.2.

[22] D. Marr and E. Hildreth, “Theory of Edge Detection,” Proceedings of the Royal Society of London. Series B. Biological Sciences, vol. 207, Feb. 1980, pp. 187 - 217.

[23] P.-W. Hsu, R.W. Prager, A.H. Gee, and G.M. Treece, “Real-Time Freehand 3D Ultrasound Calibration,” Ultrasound in Medicine & Biology, vol. 34, Feb. 2008, pp. 239-251.

[24] D.C. Barratt, B.B. Ariff, K.N. Humphries, S.A.M.G. Thom, and A.D. Hughes, “Reconstruction and quantification of the carotid artery bifurcation from 3-D ultrasound images,” *Medical Imaging, IEEE Transactions on,* vol. 23, 2004, pp. 567-583.

[25] A. Krasinski, B. Chiu, A. Fenster, and G. Parraga, “Magnetic resonance imaging and three-dimensional ultrasound of carotid atherosclerosis: Mapping regional differences,” *Journal of Magnetic Resonance Imaging*, vol. 29, 2009, pp. 901-908.

[26] E.C. Kyriacou, C. Pattichis, M. Pattichis, C. Loizou, C. Christodoulou, S.K. Kakkos, and A. Nicolaides, “A Review of Noninvasive Ultrasound Image Processing Methods in the Analysis of Carotid Plaque Morphology for the Assessment of Stroke Risk,” *Information Technology in Biomedicine, IEEE Transactions on*, vol. 14, 2010, pp. 1027-1038.

[27] F Yusoff, R Rahmat, M N Sulaiman, M H Shaharom, H Majid, “3D Based Head Movement Tracking for Incorporation in Facial Expression System”, IJCSNS International Journal of Computer Science and Network Security, VOL.9 No.2, February 2009.

[28] A. Khamene and F. Sauer, “A novel phantom-less spatial and temporal ultrasound calibration method,” *Medical Image Computing and Computer-Assisted Intervention: MICCAI ... International Conference on Medical Image Computing and Computer-Assisted Intervention,* vol. 8, no. 2, pp. 65-72, 2005.

[29] L. Antiga and D. A. Steinman, “Robust and objective decomposition and mapping of bifurcating vessels,” *Medical Imaging, IEEE Transactions on*, vol. 23, no. 6, pp. 704-713, 2004.

[30] P.-W. Hsu, R. W. Prager, A. H. Gee, and G. M. Treece, “Rapid, easy and reliable calibration for freehand 3D ultrasound,” *Ultrasound in Medicine & Biology*, vol. 32, no. 6, pp. 823-835, Jun. 2006.

[31] R. J. Housden et al., “Hybrid systems for reconstruction of freehand 3D ultrasound data,” 2007.

[32] C. Bergmeir, M. Seitel, C. Frank, R. D. Simone, H.-P. Meinzer, and I. Wolf, “Comparing calibration approaches for 3D ultrasound probes,” *International Journal of Computer Assisted Radiology and Surgery*, vol. 4, no. 2, pp. 203-213, 2008.

[33] Alexandre Krupa, “Automatic Calibration of a Robotized 3D Ultrasound Imaging System by Visual Servoing.”

[34] G. Dardenne, J. D. G. Cano, C. Hamitouche, E. Stindel, and C. Roux, “A new optimization approach for the calibration of an ultrasound probe using a 3D optical localizer,” in *Engineering in Medicine and Biology Society, 2007. EMBS 2007. 29th Annual International Conference of the IEEE*, 2007, pp. 3048-3051.

[35] Yao Rao, Li Xiaoxing and Jiang Lipei and Deng Shuangcheng and Cao Yingyu and Yao Peng and Li Xiaohong, , and , Liu Songqing, “3-D calibration method for freehand ultrasound image with high precision based on string-beads phantom,” in *Industrial Mechatronics and Automation (ICIMA), 2010 2nd International Conference on*, 2010, vol. 1, pp. 286-289.

[36] D. M. Muratore and R. L. Galloway, “Beam calibration without a phantom for creating a 3-D freehand ultrasound system,” *Ultrasound in Medicine & Biology*, vol. 27, no. 11, pp. 1557-1566, Nov. 2001.

[37] F. Lindseth, G. A. Tangen, T. Langø, and J. Bang, “Probe calibration for freehand 3-D ultrasound,” *Ultrasound in Medicine & Biology*, vol. 29, no. 11, pp. 1607-1623, Nov. 2003.

[38] T. C. Poon and R. N. Rohling, “Comparison of calibration methods for spatial tracking of a 3-D ultrasound probe,” *Ultrasound in Medicine & Biology*, vol. 31, no. 8, pp. 1095-1108, Aug. 2005.

[39] S. Tong, D. B. Downey, H. N. Cardinal, and A. Fenster, "A three-dimensional ultrasound prostate imaging system," *Ultrasound in Medicine & Biology*, vol. 22, no. 6, pp. 735-746, 1996.

[40] A. Fenster, N. Cardinal, S. Tong, and D. B. Downey, "Development and evaluation of a 3D ultrasound imaging system," in *IMTC/98 Conference Proceedings. IEEE Instrumentation and Measurement Technology Conference. Where Instrumentation is Going (Cat. No.98CH36222), 18-21 May 1998,* New York, NY, USA, 1998, vol. 1, pp. 562-5.

[41] T. L. Elliot, D. B. Downey, S. Tong, C. A. McLean, and A. Fenster, "Accuracy of prostate volume measurements in vitro using three-dimensional ultrasound," *Academic Radiology*, vol. 3, no. 5, pp. 401-406, May. 1996.

[42] J. N. Welch et al., "Real-time freehand 3D ultrasound system for clinical applications," in *Medical Imaging 2001: Visualization, Display, and Image-Guided Procedures, 18-20 Feb. 2001,* USA, 2001, vol. 4319, pp. 724-30.

[43] M. S. Pattichis and M. B. Goens, with Honggang Yu, "Multi-view 3D reconstruction with volumetric registration in a freehand ultrasound imaging system," in *Medical Imaging 2006: Ultrasonic Imaging and Signal Processing, 12 Feb. 2006,* USA, 2006, vol. 6147, pp. 614706-1.

[44] A. K. Hamou and M. R. El-Sakka, "A novel segmentation technique for carotid ultrasound images," in *Acoustics, Speech, and Signal Processing, 2004. Proceedings. (ICASSP '04). IEEE International Conference on*, 2004, vol. 3, pp. iii-521-4 vol.3.

[45] F. Molinari, G. Zeng, and J. S. Suri, "A state of the art review on intima-media thickness (IMT) measurement and wall segmentation techniques for carotid ultrasound," *Computer Methods and Programs in Biomedicine*, vol. 100, no. 3, pp. 201-221, Dec. 2010.

[46] L. Goubergrits, K. Affeld, J. Fernandez-Britto, and L. Falcon, "Geometry of the Human Common Carotid Artery. A Vessel Cast Study of 86 Specimens," *Pathology - Research and Practice*, vol. 198, no. 8, pp. 543-551, 2002.

[47] M. Naghavi et al., "From Vulnerable Plaque to Vulnerable Patient," *Circulation*, vol. 108, no. 14, pp. 1664 -1672, Oct. 2003.

[48] B. Lal et al., "Noninvasive Identification of the Unstable Carotid Plaque," *Annals of Vascular Surgery*, vol. 20, no. 2, pp. 167-174, Mar. 2006.

[49] Spence JD, Eliasziw M, DiCicco M, Hackam DG, Galil R, Lohmann T. Carotid plaque area: a tool for targeting and evaluating vascular preventive therapy. Stroke. 2002;33(12):2916-2922.

[50] O. Joakimsen, K. H. Bønaa, and E. Stensland-Bugge, “Reproducibility of Ultrasound Assessment of Carotid Plaque Occurrence, Thickness, and Morphology□ : The Tromsø Study,” *Stroke*, vol. 28, no. 11, pp. 2201 -2207, Nov. 1997.

[51] M. L. Bots, P. G. H. Mulder, A. Hofman, G.-A. van Es, and D. E. Grobbee, “Reproducibility of carotid vessel wall thickness measurements. the rotterdam study,” *Journal of Clinical Epidemiology*, vol. 47, no. 8, pp. 921-930, Aug. 1994.

[52] J. Persson, L. Stavenow, J. Wikstrand, B. Israelsson, J. Formgren, and G. Berglund, “Noninvasive quantification of atherosclerotic lesions. Reproducibility of ultrasonographic measurement of arterial wall thickness and plaque size,” *Arteriosclerosis, Thrombosis, and Vascular Biology*, vol. 12, no. 2, pp. 261 -266, Feb. 1992.

[53] N. Pagoulatos, D. R. Haynor, and Y. Kim, “A fast calibration method for 3-D tracking of ultrasound images using a spatial localizer,” *Ultrasound in Medicine & Biology*, vol. 27, no. 9, pp. 1219-1229, Sep. 2001.

[54] L. Barber, R. Barrett, and G. Lichtwark, “Validation of a freehand 3D ultrasound system for morphological measures of the medial gastrocnemius muscle,” *Journal of Biomechanics*, vol. 42, no. 9, pp. 1313-1319, Jun. 2009.

[55] A. M. Goldsmith, P. C. Pedersen, and T. L. Szabo, “An inertial-optical tracking system for portable, quantitative, 3D ultrasound,” in *IEEE Ultrasonics Symposium, 2008. IUS 2008*, 2008, pp. 45-49.

[56] G. Treece, R.W. Prager, and A.H. Gee. The Stradwin 3D Ultrasound Acquisition and Visualization System. http://www.eng.cam.ac.uk/~rwp/stradwin/

[57] D. D. B. Carvalho et al., “Estimating 3D lumen centerlines of carotid arteries in free-hand acquisition ultrasound,” International Journal of Computer Assisted Radiology and Surgery, Jun. 2011.

[58] R. A. Chaer, B. DeRubertis, S. Patel, S. C. Lin, C. K. Kent, and P. L. Faries, "Current management of extracranial carotid artery disease," Reviews on Recent Clinical Trials, vol. 1, pp. 293-301(9), September 2006.

[59] D. Lloyd-Jones et al., "Heart disease and stroke statistics-2010 update: A report from the American Heart Association," Circulation, vol. 121, no. 7, pp. e46-215, 2010.

[60] C. J. L. Murray and A. D. Lopez, "Mortality by cause for eight regions of the world: Global burden of disease study," The Lancet, vol. 349, pp. 1269-1276, May 1997.

[61] D. Kleut, M. Jovanović and B. Reljin, 3D visualization of MRI images using Matlab. *Journal of Automatic Control*, 16 (2006), pp. 1–3.

[62] American Stroke Association (Updated: Fri, 4 Nov 2011). Impact Of Stroke [Online]. Available: http://www.strokeassociation.org/STROKEORG/AboutStroke/Impact-of-Stroke_UCM_310728_Article.jsp#.TtPu_VZc0dY

[63] Incidence and Prevalence: 2006 Chart Book on Cardiovascular and Lung Diseases. Betheseda, MD: National Heart, Lung, and Blood Institute. 2006. Cited in Veronique L. Roger et. al., "Heart disease and stroke statistics--2011 update: A report from the American Heart Association," Circulation, 123, December 15, 2010. [Online]. Available: http://circ.ahajournals.org/content/123/4/e18.full.pdf. [28 Nov 2011].

[64] Petras, Ivo, Orthogonal Linear Regression in 3D-space by using Principal Components Analysis (File ID: #12395) [Online]. Available: http://www.mathworks.com/matlabcentral/fileexchange/12395

[65] G. G. Ferguson et al., “The North American Symptomatic Carotid Endarterectomy Trial: Surgical Results in 1415 Patients,” Stroke, vol. 30, no. 9, pp. 1751 -1758, 1999.

[66] L. Mercier, T. Langø, F. Lindseth, and L. D. Collins, “A review of calibration techniques for freehand 3-D ultrasound systems,” Ultrasound in Medicine & Biology, vol. 31, no. 2, pp. 143-165, Feb. 2005.

Curriculum Vitae

Rumman Mahmud received her Bachelor of Science in Computer Engineering from George Mason University in 2002. She has six years of experience in consultation for Federal Information Processing Standard (FIPS) 140-2 and performing cryptographic algorithm testing. Ms. Mahmud has rejoined George Mason University in 2008 to pursue Masters in Computer Engineering. Her interests involve Field Programmable Gate Array (FPGA) implementations and applications of ultrasound imaging.